growing bacteria in minimal medium containing $^{15}NH_4Cl$ with or without [$^{13}C_6$]glucose. Uniformly $^{15}N/^{13}C$-labeled and fractionally deuterated protein sample was prepared using medium containing 60% ^2H_2O. The NHE1-CHP1 complex was purified using a standard Ni-NTA affinity column protocol (Qiagen). Further purification was performed by gel filtration using Superdex 200 (GE Healthcare). NMR samples contained 0.5–0.9 mM protein in 50 mM Tris-d_7 buffer (pH 6.9), 1 mM dithiothreitol-d_{10}, 30 mM KCl in $H_2O/^2H_2O$ (9:1) or ^2H_2O.

NMR Spectroscopy—NMR data were recorded at 37 °C on Bruker AVANCE 500 and DRX 800 NMR spectrometers. Resonance assignments for ^{1}HN, ^{15}N, $^{13}C\alpha$, $^{13}C\beta$, and $^{13}C'$ nuclei for the CHP1-NHE1 complex were obtained through the following ^{2}H-decoupled, triple resonance spectra applied to a fractionally deuterated $^{15}N/^{13}C$-labeled sample: three-dimensional HNCACB/HN(CO)CACB (24) and three-dimensional HN(CA)CO/HNCO experiments (25, 26). Side-chain ^{1}H and ^{13}C resonances were assigned on a fully protonated sample or a fractionally deuterated $^{15}N/^{13}C$-labeled sample using three-dimensional C(CO)NH, three-dimensional H(CCO)NH, four-dimensional HC(CO)NH, and three-dimensional HCCH TOCSY (27–29). Stereospecific assignment of leucine and valine methyl groups were obtained from a Constant Time-$^1H/^{13}C$ HSQC spectrum of a 15% ^{13}C-labeled sample (30). $^1H\alpha$ and $^1H\beta$ resonance assignments were supplemented with three-dimensional H(CACO)NH (31), ^{15}N-edited TOCSY-HSQC (32), and three-dimensional HBHA(CBCACO)NH (33). Aromatic resonances of both NHE1 and CHP1 were mainly assigned using three-dimensional ^{13}C-aromatic-edited/^{15}N-separated NOESY-HSQC, three-dimensional ^{13}C-edited NOESY, ^{1}H-^{1}H TOCSY, and NOESY experiments (32). The assignment was verified using the Constant Time-$^1H/^{13}C$ HSQC spectrum of a 15% ^{13}C-labeled sample (30). The following NOESY spectra were recorded for the protonated sample and used to generate distance restraints for structure calculations: three-dimensional ^{15}N-edited NOESY (80-ms mixing time), three-dimensional ^{13}C-edited NOESY (80-ms mixing time), and two-dimensional ^{1}H NOESY (80-ms mixing time). Slowly exchanging amide protons were identified from a series of two-dimensional ^{15}N HSQC spectra recorded after the H_2O buffer was replaced with ^2H_2O buffer. All NMR spectra were processed using NMRPipe/NMRDraw (34) analyzed using SPARKY (35).

Structure Calculations—Intramolecular and intermolecular distance constraints were identified in the three-dimensional $^{15}N/^{13}C$-separated NOESY spectra using a $^{15}N/^{13}C$-labeled NHE1-CHP sample with mixing times of 80 ms. Backbone hydrogen bond restraints within regular secondary structure elements that were consistent with backbone amide hydrogen/deuterium exchange data were included in the structure calculations. The initial structure calculations were performed by iterative automated assignment of the NOE spectra using CANDID (36) in addition to manually assigned NOE-derived distance restraints. The restraints, leading to converged structures, were subsequently utilized for the iterative automated assignment of all spectra including aromatic residues using CANDID. Finally refinement of the structures (including two Ca^{2+} ions) using XPLOR-NIH (version 2.96) was performed (37). The final structure calculations used a total of 4022 NOE-derived distance restraints obtained from the manual and the CANDID-assisted assignments from the ^{15}N- or ^{13}C-edited NOE data. A total of 100 simulated annealing structures were calculated, and 20 structures were selected that possessed no NOE violations greater than 0.5 Å and no dihedral violations greater than 5°. Final structures were evaluated using the program ProcheckNMR (38). Structures and figures were drawn using MOLMOL (39), GRASP (40), and Chimera (41).

Mutagenesis and GST Pulldown Assay—For the binding analyses, CHP1 was expressed as a fusion protein with GST in *E. coli*, which was then subcloned into modified pGEX6P-3 (Novagen) (42). Site-directed mutant proteins were prepared using the QuikChange kit (Stratagene). DNA sequencing confirmed the mutations. Vectors were transformed into BL21(DE3)star (Invitrogen). Cells were grown at 37 °C and then induced with 1 mM isopropyl 1-thio-β-D-galactopyranoside for 12 h at 20 °C. Harvested cells were disrupted via sonication in HEPES (pH 8.0) containing 10% glycerol, 10% sucrose, 1 mM dithiothreitol, and 30 mM KCl. The GST-CHP1 fusion protein was purified using glutathione-Sepharose (GE Healthcare) and a standard protocol except that the equilibrium buffer was changed to 50 mM HEPES buffer (pH 8.0) containing 10% glycerol, 1 mM dithiothreitol, and 30 mM KCl, and the column was washed extensively with 20 mM CHAPS. The effect of mutation on the binding of CHP1 to NHE1 peptides was characterized using a GST pulldown assay. Synthetic NHE1 peptide (residues 514–545 including a hexahistidine sequence at the C terminus) was purchased from Greiner Japan (Tokyo, Japan). Briefly wild-type and CHP1 mutant GST fusion proteins, in addition to GST alone, were incubated for 30 min at 20 °C with NHE1 peptide in binding buffer containing 50 mM HEPES (pH 7.5), 20 mM CHAPS, 10% glycerol, 1 mM Pefabloc, and 1 mM dithiothreitol. GST protein-bound Sepharose beads were washed extensively with binding buffer. Proteins were resolved by 12% NuPAGE (Invitrogen) and blotted onto membranes, and then His-NHE1 was analyzed with Ni-NTA-conjugated alkaline phosphatase (Promega) and Western Blue substrate (Promega). Quantification was represented as the average value of experiments performed in triplicate.

RESULTS AND DISCUSSION

Structure Determination—To better understand the mechanism pertaining to CHP1-regulated NHE1 activity, the solution structure of unmyristoylated CHP1 complexed with the cytoplasmic region (503–545) of NHE1 was determined by NMR spectroscopy. Our structural studies were initially hampered by the fact that NHE1-free CHP1 tended to aggregate during NMR measurements, and the CHP1-unbound cytoplasmic region (503–545) of NHE1 readily degraded during the expression and purification steps. Consequently NMR structural analysis of co-expressed and co-purified samples was undertaken. Co-expression of CHP1 and NHE1-(503–545) produced a stable complex for structural studies and showed no significant degradation and aggregation for several weeks.

The ^{1}H-^{15}N HSQC spectrum of NHE1-unbound CHP1 displays many broadened peaks presumably due to formation of a dimer, multimer, or an equilibrium between these states in solution. In contrast, the HSQC spectrum of ^{15}N-labeled CHP1

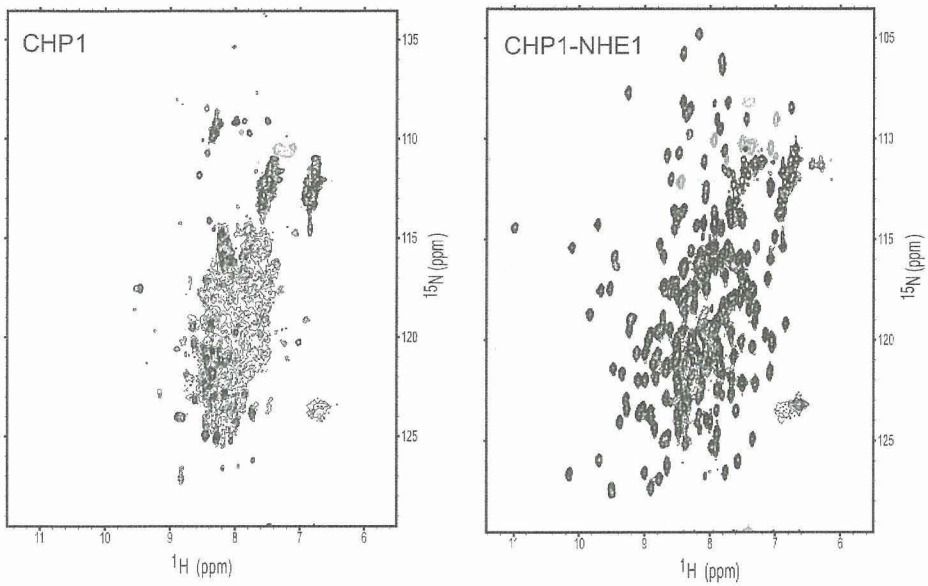

FIGURE 2. **^{1}H-^{15}N HSQC spectra of ^{15}N-labeled NHE1-free CHP1 (*left image*) and ^{15}N-labeled NHE1-(503–545)-CHP1 complex (*right image*).** These spectra were obtained with 0.3 mM samples at pH 6.9 and 37 °C recorded on the AVANCE 500.

TABLE 1

Structural statistics for NHE1-CHP1

These statistics represent an ensemble comprising 20 of the lowest energy structures obtained from 150 starting structures. Structure calculations were performed using XPLOR-NIH version 2.9.6.

Total number of distance constraints	4242
Long range ($\|i-j\|>4$)	589 (inter: 134)
Middle range ($\|i-j=2,3,4$)	874
Short range ($\|i-j\|=1$)	1038
Intraresidue	1521
Hydrogen bond constraints (including Ca^{2+} coordination restraints)	110 × 2
Dihedral constraints	
ϕ, φ	105, 105
$\chi 1$	17
r.m.s. deviation from experimental constraints[a]	
Distance (Å)	$0.0288 \pm 7 \times 10^{-4}$
Angle (°)	$0.44 \pm 3 \times 10^{-2}$
r.m.s. deviation from idealized covalent geometry	
Bonds (Å)	$0.00248 \pm 6 \times 10^{-5}$
Angles (°)	$0.360 \pm 6 \times 10^{-3}$
Impropers (°)	$0.31 \pm 1 \times 10^{-2}$
XPLOR energy terms (kcal/mol)[b]	
E_{bond}	23 ± 1
E_{angle}	138 ± 5
E_{imp}	28 ± 2
$E_{vdw(LJ)}$	$-6.6 \times 10^{2} \pm 0.2 \times 10^{2}$
PROCHECK Ramachandran plot (185–254)	
Residues in most favored regions (%)	78.6
Residues in additional allowed regions (%)	18.1
Residues in generously allowed regions (%)	2.9
Residues in disallowed regions (%)	0.4
r.m.s. deviation of mean structure derived from 30 calculated structures	
Backbone (10–92, 108–192, 516–538) (Å)	0.53
All heavy (10–92, 108–192, 516–538) (Å)	1.15

[a] None of these structures exhibited distance violations >0.5 or dihedral angle violations >5°.

[b] $E_{vdw(LJ)}$ represents the Lennard-Jones energy of the XPLOR energy terms.

complexed with NHE1 is well dispersed with favorable line shapes (Fig. 2), suggesting that the complex essentially adopts an ordered monomeric structure in solution.

Our target complex was ~27 kDa in size, assuming a 1:1 complex of CHP1 (22 kDa) and NHE1 (5 kDa). This represented a relatively large molecular weight in terms of conventional NMR studies. Consequently utilization of triple labeling (^{2}H, ^{13}C, and ^{15}N) and the recently developed computational methodology, CANDID, was extremely helpful in the structure determination. Sequential backbone assignments and most side-chain assignments were obtained from a 60% ^{2}H/^{15}N/^{13}C-labeled sample using standard triple resonance experiments. Missing ^{1}H resonances were supplemented using heteronuclear three-dimensional NOESY experiments with ^{15}N/^{13}C-labeled samples. Resonance assignments of methyl groups were carefully confirmed in a stereospecific manner using two-dimensional Constant Time HSQC spectra recorded for a 15% randomly enriched ^{13}C sample. Methyl groups for 18 of 24 leucines and nine of 11 valines were stereospecifically assigned. Aromatic ring proton assignments, essential for delineating hydrophobic core and protein-protein interactions, were obtained using two-dimensional TOCSY, two-dimensional NOESY, two-dimensional HCCH(arom) TOCSY, and three-dimensional ^{13}C(arom)-edited ^{15}N-separated NOESY experiments.

NMR spectra including the three-dimensional ^{13}C-edited NOESY spectrum used to monitor inter/intramolecular ^{1}H-^{1}H NOEs were of adequate quality to pursue a structural determination of the NHE1-CHP1 complex. Use of partial deuteration and the almost complete resonance assignment of methyl groups forming the hydrophobic core facilitated an initial determination of the overall protein fold. A high resolution structure was subsequently obtained using CANDID for automated assignments, which included the use of ambiguous NOEs from ^{15}N- and ^{13}C-edited NOESY experiments recorded for ^{15}N- or ^{15}N/^{13}C-labeled protein samples. An iterative approach was used for assigning NOEs in addition to the manually assigned unambiguous NOEs. The solution structure of the CHP1-NHE1 complex was determined from a total of over 4000 NMR-derived restraints, including 134 intermolecular distance restraints (Table 1). The ensemble of 20 structures in excellent agreement with a large body of experimental data were well defined (Fig. 3*A*). The r.m.s. deviations of backbone and heavy atoms over residues 518–537 of NHE1 and residues 10–92 and 108–193 of CHP1 were 0.53 and 1.15 Å, respectively. Of the NMR structures determined, the one with the smallest total energy was selected as representative for further discussion. The complex is predominantly α-helical, and the CHP1 helices constitute a cleft. A helix of the cytoplasmic region of NHE1 associates with CHP1 in 1:1 stoichiometry via the cleft (Fig. 3, *A* and *B*).

Structure of NHE1—NHE1 forms a five-turn amphipathic helix composed of residues 518–537. Orientation of the NHE1 helix is well defined relative to CHP1, consistent with the large

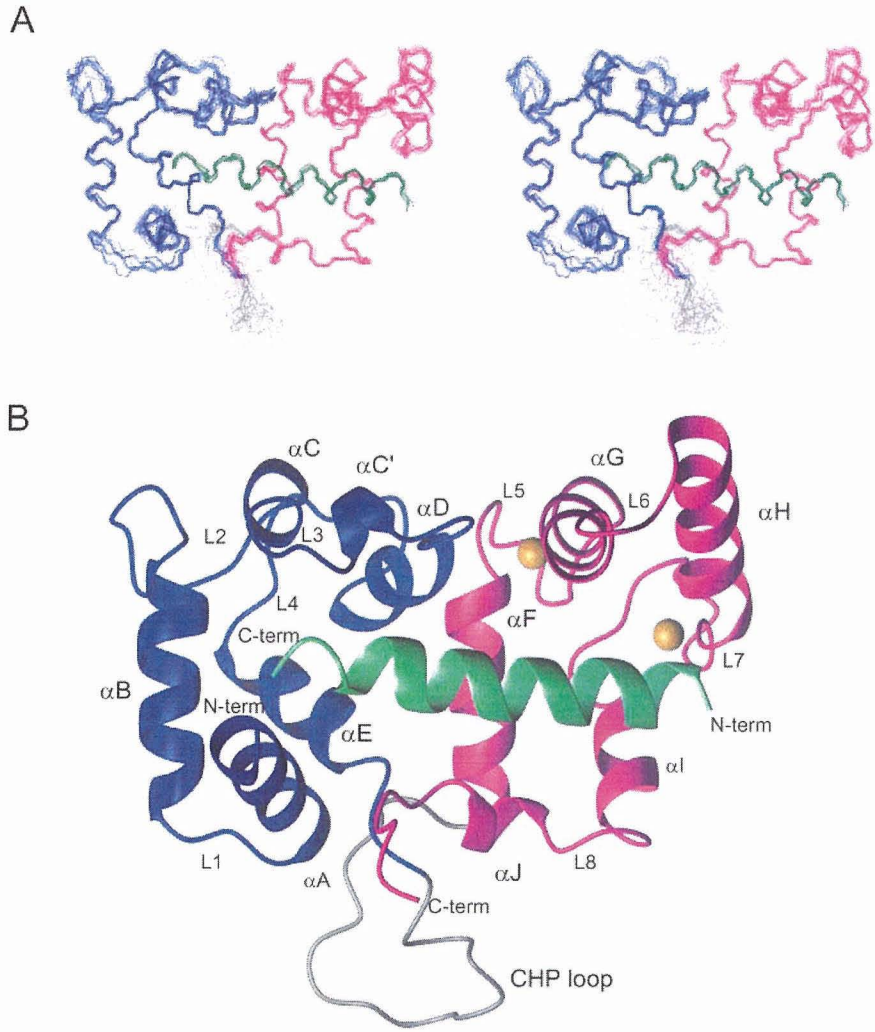

FIGURE 3. **Solution structure of the NHE1-CHP1 complex.** *A*, stereoview of the backbone superpositions of the final 20 simulated annealing structures of the NHE1-CHP1 complex. *B*, ribbon drawing of the representative NHE1-CHP1 structure complex. *A* and *B*, residues 517–538 of NHE1 and 10–192 of CHP1 are shown. The N- and C-terminal domains of CHP1 are colored in *blue* and *magenta*, respectively, and the CHP loop is colored in *gray*. NHE1 is shown in *green*. Ca^{2-} ions are shown by *gold spheres*.

number of intermolecular NOEs detected between CHP1 and NHE1 (Table 1 and Fig. 3*A*). The N-terminal half of the helix (residues 518–530) binds to the C-terminal domain of CHP1, and the C-terminal half of the helix (residues 531–537) binds to the N-terminal domain of CHP1 (Fig. 4*A*). Side-chain conformations of the helix are also well defined particularly for apolar residues that make extensive contacts with CHP1. For example, NMR spin-echo difference $^3J_{NC\gamma}$ and $^3J_{C'C\gamma}$ experiments, which bring about $\chi 1$ rotamer information of aromatic side chain, showed that the His-523 and Phe-526 adopted $g+$ and t conformations, respectively. The helix exhibits amphipathic character in which the bulky hydrophobic residues Ile-518, Ile-522, His-523, Phe-526, Leu-527, Leu-530, Leu-531, Ile-534, and Ile-537 are clearly confined to one side, and hydrophilic residues are exposed at the other side (Fig. 4*B*). The hydrophobic residues form a continuous apolar surface (Fig. 4*B*). The main-chain and side-chain conformations of residues preceding and following the helix, residues 503–517 and 538–545, respectively, are poorly defined in the NMR structure because of the absence of medium and long range NOEs involving these regions. The narrow resonance linewidths, chemical shift index, and steady state $\{^1H\}$-^{15}N heteronuclear NOE suggest that these regions are unstructured in the complex.

Structure of CHP1—CHP1 is composed of 10 α-helices and a long loop folded into two globular regions representing the N- and C-terminal domains (Fig. 3*B*). The secondary structure consists of αA (residues 11–22), αB (residues 26–37), αC (residues 48–51), αD (residues 64–70), αE (residues 80–88), αF (residues 111–122), αG (residues 132–143), αH (residues 149–162), αI (residues 174–180), and αJ (residues 185–188) (Figs. 1*B* and 3*B*). The N-terminal domain consists of ancestral EF-hands, EF-1 and EF-2, that do not bind calcium under physiological conditions. The EF-1 hand includes helix αB, loop L2, and helix αC followed by loop L3 to the second EF-hand that includes helix αD, loop L4, and helix αE (Figs. 1*B* and 3*B*). A long loop region consisting of residues 93–110 connects the N- and C-terminal domains. Because this characteristic long insertion is not found in calcineurin B (Figs. 1*B* and 3, *A* and *B*), we refer to this long loop as the CHP loop. The absence of medium and long range NOEs, a chemical shift index, and $\{^1H\}$-^{15}N heteronuclear NOE value indicate that this region is flexible in solution. The first EF-hand in the C-terminal domain includes helix αF, loop L5, and helix αG followed by loop L6 and the second EF-hand that consists of helix αH, loop L7, and helix αI (Figs. 1*B* and 3*B*).

The four CHP1 EF-hands form a deep hydrophobic pocket, which constitutes the interaction surface for the NHE1 amphipathic α-helix. CHP1 binds to the apolar side of NHE1 with the four EF-hands through a side-by-side manner (Fig. 4*A*). This contrasts with the well known canonical CaM-target binding mode that represents a wrap-around manner in which two pairs of EF-hands bind to the target IQ motif helix on opposite sides to each other (43, 44).

Although there is modest sequence similarity between CHP1 and CaM, it should be noted that the latter interacts with a large number of proteins with various interaction modes including canonical 1:1 binding and non-canonical 1:1, 1:2, and 2:2 binding (43, 44). It has been suggested that the observed binding versatility of CaM could be derived from the variable positioning of the two domains, linked by a flexible linker, that can

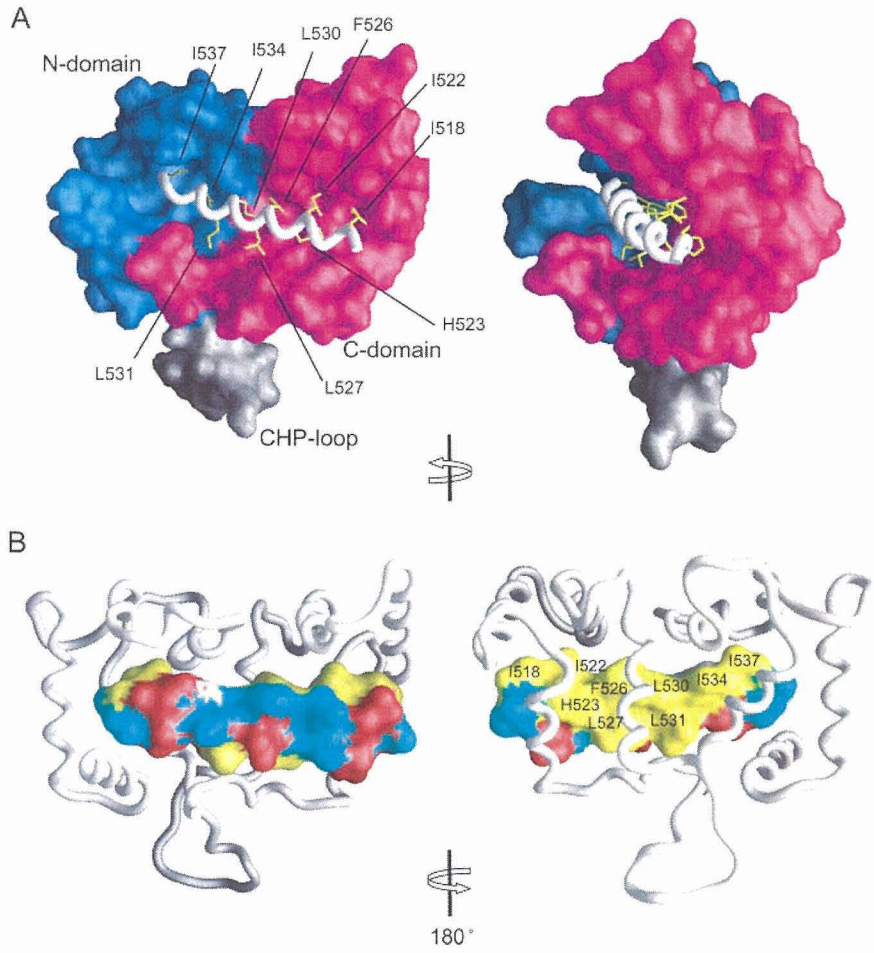

FIGURE 4. **Molecular surface of the NHE1-CHP1 complex.** *A*, molecular surface of CHP1 and backbone *tube* representation of NHE1 with *yellow stick* that shows the hydrophobic side chains. The N- and C-terminal domains of CHP1 are colored in *blue* and *magenta*, respectively. *B*, molecular surface of NHE1 and backbone *tube* representation of CHP1. Hydrophobic, acidic, and polar residues are colored in *yellow*, *red*, and *blue*, respectively.

accommodate different targets. Although target multiplicity has been reported in the case of CHP1, it seems to possess more limited binding modes than CaM. One notable feature of CHP1 that illustrates its difference to CaM has to do with the interdomain interaction. This interaction restricts domain orientation, a phenomenon absent in CaM. In our CHP1 structure, residue Leu-62 of the N-terminal domain participates in a hydrophobic interaction with residues Val-138 and Met-141 of the C-terminal domain, and residue Ala-69 of the N-terminal domain interacts with residue Leu-122 of the C-terminal domain. A side-by-side interaction mediated by four EF-hands has also been reported to take place with voltage-gated potassium channel (Kv)-interacting protein (KChIP) (45) and with CNA-CNB (46, 47) (Fig. 5*A*).

The atomic r.m.s. difference of well fitted parts between CHP1 complexed with NHE1 and CNB complexed with CNA (Protein Data Bank code 1AUI) is 2.7 Å, indicating that the fit is not very good, although the topology is identical with a high Z-score of 11.8 from a distance matrix alignment (DALI) search. The r.m.s. deviation value improves to 1.7 Å when only the N-terminal domains are superimposed, and it is 1.8 Å when only the C-terminal domains are superimposed. This indicates that the higher r.m.s. deviation for both domains originates from an interdomain swiveling between NHE1-CHP1 and CNA-CNB, although both proteins bind cognate targets in a side-by-side manner. Similarly domain swiveling was observed between NHE1-bound and NHE-free CHP1. Swiveling of the N- and C-terminal domains could create a binding surface for cognate targets.

Comparison with Other EF-hands—It is interesting to note that both EF-1 and EF-2 adopt an open conformation in NHE1-bound CHP1 without Ca^{2+}. This is especially evident when comparing the angles between the EF-hand helices. In Fig. 5*B*, a graphical view of the interhelical angles between the first and second helices of EF-1 and EF-2 of apoCaM (a typical closed conformation), Ca^{2+}-CaM (a typical open conformation, CNB), KChIP1, NHE1-bound CHP1, and NHE1-free CHP1 is displayed using a vector geometry mapping method (48, 49). The first helices of the EF-hands are superimposed along the *z* axis, and the spatial localization of the second helices are shown as a *cylinder*. This indicates that both EF-1 and EF-2 of NHE1-bound CHP1 adopt an open conformation, whereas EF-1 and EF-2 of NHE1-free CHP1 adopt an open and semiopen conformation, respectively (Fig. 5*B* and supporting information S1). This implies that EF-1 and EF-2 adopt a constitutively open conformation. However, it should be noted that the hydrophobic cleft of the N-terminal domain of free CHP1, as revealed by the crystal structure, is plugged by additional linker residues (Leu-Ala-Ala-Ala-Leu-Glu-His) (23) derived from the expression vector, partly mimicking the NHE1 helix (Fig. 5*A*). Binding of the vector-derived linker might have facilitated adoption of the open and semiopen conformations of EF-1 and EF-2, respectively. Therefore, the possibility of a "closed to open" conformational transition of EF-1 and EF-2 remains to be evaluated.

The binding of EF-hands in an open conformation without Ca^{2+} to target molecules has been found following crystal structure investigations of a Kv-KChIP1 in which the Kv fragment is covalently linked to the C terminus of KChIP1 (45). In this case, the Kv fragment binds to EF-1 and EF-2 of the N-terminal domain of KChIP1 through hydrophobic interactions (Fig. 5*A*). Of particular note, KChIP1 forms a dimer utilizing the surface formed by the Kv peptides and helix 10 of the C-terminal domain of KChIP1 in contrast to NHE1-CHP1, which exists as a monomer (Fig. 5*C*). The interhelix angles of EF-1 and EF-2

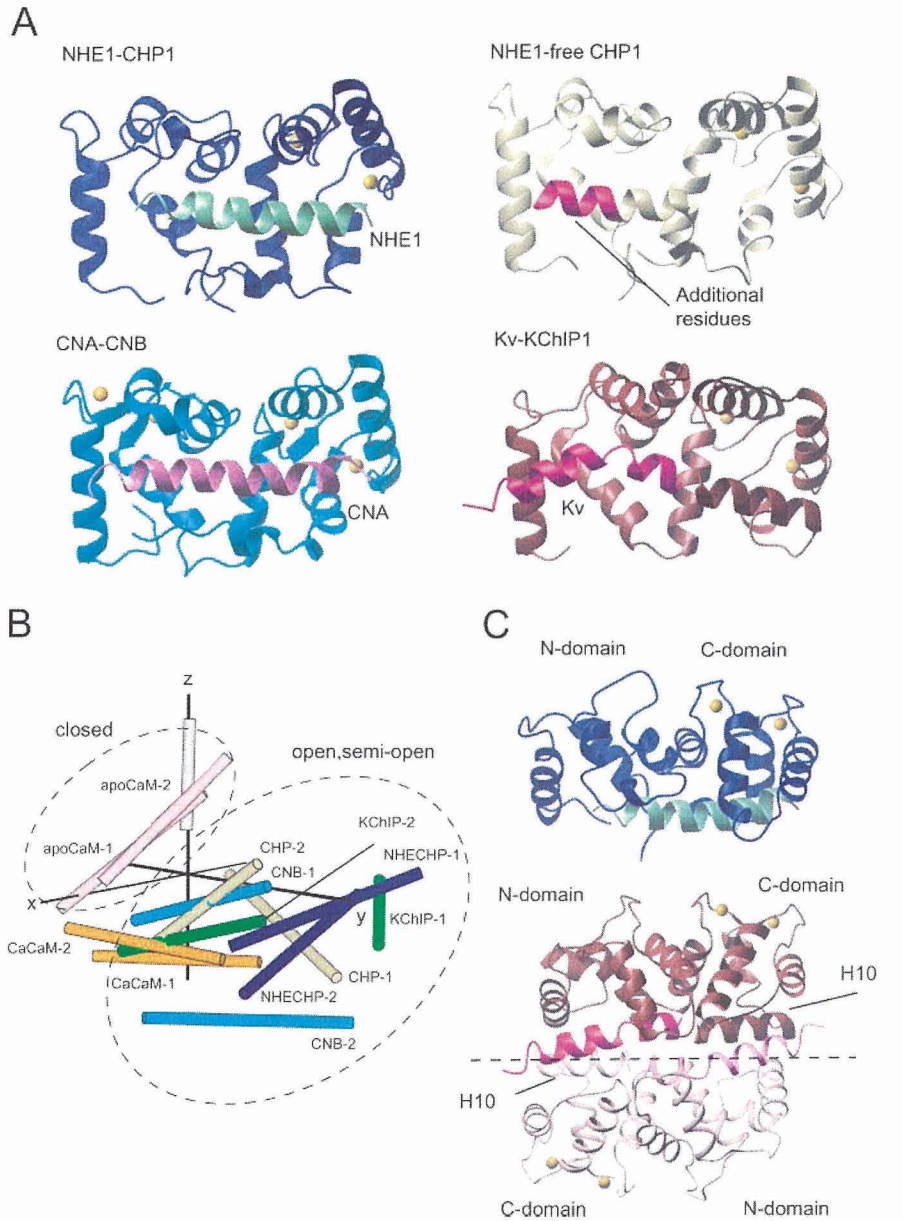

FIGURE 5. **Structure comparisons.** *A*, ribbon representation of NHE1-CHP1, rat NHE1-free CHP1 (2CT9) in which additional residues from the expression vector interacting with the N-terminal domain (LAAALEH) are depicted in *magenta*, CNA-CNB (1AUI), and Kv-KChIP1 (1S6C). Protein Data Bank entries are shown in parentheses. *B*, vector geometry mapping of EF-1 and EF-2 apocalmodulin, Ca^{2+}-calmodulin, calcineurin B, Kv-KChIP1, NHE1-bound CHP1, and NHE1-free CHP1 are denoted as *"apoCaM," "CaCaM," "CNB," "KChIP," "NHECHP,"* and *"CHP,"* respectively. *Hyphenated numbers 1* and *2* denote EF-1 and EF-2, respectively, for each protein. *C*, comparison of the KChIP1 dimer and CHP1 structures colored in *brown* and *blue*, respectively. Bound Kv and NHE1 are colored in *pink* and *green*, respectively. The dimer interface of KChIP1 is shown as a *dashed line*, and one molecule of the dimer is shown in *light colors*. KChIP1 and CHP1 are depicted in the same orientation. In *A* and *C*, the N- and C-terminal regions, αA, and the CHP loop of CHP1 are not shown in the comparison for reasons of clarity.

are 82° and 72°, respectively (supporting information S1), which are slightly larger than those of CHP1. A dimeric interaction in addition to binding of the Kv fragment may contribute to broadening of the cleft constituted by EF-1 and EF-2.

CHP1 shares 18% sequence identity with KChIP1, and the folding topology is almost identical (Fig. 5*A*). However, the target recognition mechanism differs from that of KChIP1 as judged from the determined structures. KChIP1 belongs to the extensively studied NCS1 family, which act as important regulators of various functions among certain higher eukaryotes (50). We propose that the NHE1-CHP1 interaction represents a novel binding mode utilized throughout the four-EF-hand proteins, which constitute a distinct subfamily to the NCS1 family. Furthermore detailed comparison of the binding mode of CHP1 and CNB will be presented below.

The CHP1-NHE1 Interface—The protein-protein interface consists of an extensive hydrophobic concave CHP1 undersurface and an apolar NHE1 surface. The concave undersurface spans both the N- and C-terminal domains of CHP1. The total surface area buried at the interface is 2338 $Å^2$, slightly smaller than the value of 2625 $Å^2$ for the interface between CNA and CNB (Protein Data Bank code 1AUI). Approximately more than 90% of the total buried surface area between NHE1 and CHP1 is hydrophobic, similar to the complexed structure of CNA and CNB.

The interface formed between NHE1 and CHP1 includes methyl-containing and aromatic hydrophobic residues. The residues of the N-terminal domain of CHP1, Ala-69, Phe-90, Ile-66, Thr-86, Leu-87, Phe-35, and Leu-54, comprise a hydrophobic cleft that interacts with the apolar surface formed by the side chains of NHE1 residues Leu-530, Ile-534, and Ile-537. Additionally the side chain of NHE1 Leu-531 expands the hydrophobic area interacting with CHP1 Phe-90 (Fig. 6*A*). The C-terminal domain residues of CHP1, Ala-163, Thr-159, Leu-139, Leu-135, Tyr-122, Phe-176, Ile-171, Phe-117, Ala-118, and Leu-121, constitute a continuous hydrophobic cleft that interacts with the N-terminal portion of NHE1 helix residues Ile-518, Ile-522, and Phe-526, which protrude at the apolar side. NHE1 residues Leu-527 and His-523 make additional hydrophobic contact with CHP1 residues Tyr-122, Phe-176, and Val-185 (Fig. 6*A*). These interface-forming hydrophobic residues are well conserved within NHE and CHP isoforms, reflecting the importance of these interactions (Fig. 1*B*). Furthermore the acidic side chain of Asp-528 at the center of NHE1 helix seems to form a salt bridge with the basic side

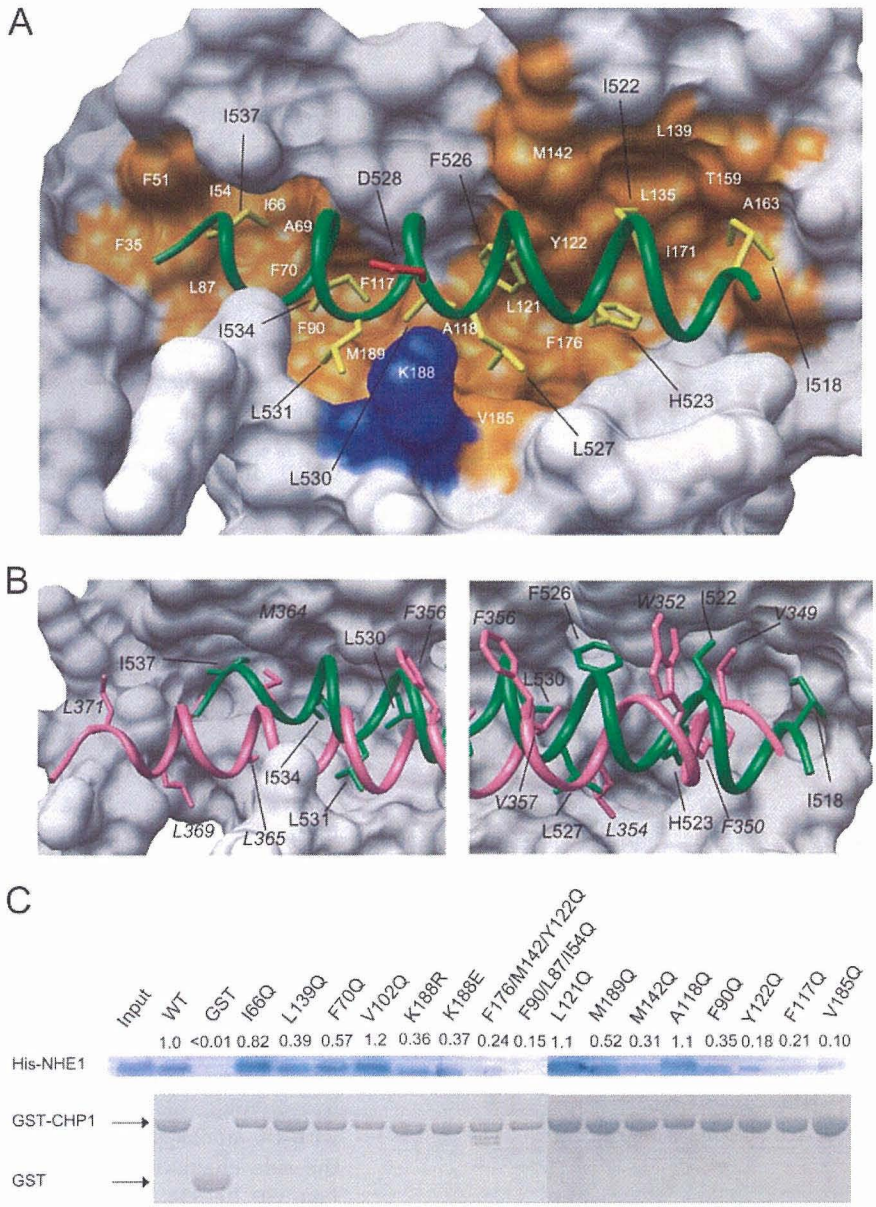

FIGURE 6. **Noncovalent interactions at the NHE1-CHP1 interface and contribution to the overall stability of the complex.** *A*, molecular surface of CHP1 and backbone *tube* representation of NHE1 with *yellow* and *red sticks* that show hydrophobic and acidic side chains, respectively. Hydrophobic and basic surface residues of CHP1 are colored in *orange* and *blue*, respectively. *B*, superposition of NHE1-CHP1 and CAN-CNB (Protein Data Bank code 1AUI). NHE1 and CNA are shown in *green* and *magenta*, respectively, and the molecular surface of only CHP1 is depicted for clarity. Complex-forming hydrophobic residues of NHE1 and CNA are shown as *sticks* and are labeled. CNA residues are represented in *italics*. The *left-hand image* and the *right-hand image* are close-up views of the N- and C-terminal domains. *C*, binding of His-NHE1 peptide to GST-CHP1 mutants in an *in vitro* pulldown assay. Bound peptide was separated via SDS-PAGE, blotted to a membrane, and then visualized using Ni-NTA-conjugated alkaline phosphatase (*top*). The amount of GST-CHP1 mutant used was estimated by Coomassie Blue staining (*bottom*) for calibration. The binding of NHE1 peptide to GST-CHP1 mutants was quantified and expressed as a ratio of binding of wild-type protein at the *top* of the gel images.

chain of CHP1 Lys-188. The presence of this interaction was observed in 10 of the final 20 NMR structures derived using the MONSTER server (51), which identifies interacting residues and assigns the nature of those interactions based on the structure. These residues are also conserved (Figs. 1, *A* and *B*, and 6*A*).

NHE1 binding orientation relative to CHP1 is probably established by surface complementarity that comprises the hydrophobic surfaces of NHE1 and CHP1. NHE1 side chains of Ile-534 and Ile-537 protrude into the shallow cleft made by the CHP1 N-terminal domain. Meanwhile NHE1 aromatic side chains of His-523 and Phe-526 protrude into the deep cleft of the CHP1 C-terminal domain (Fig. 6*A*). This deep cleft allows enough space so that they can interact with the bulky side chains of NHE1. The difference between the shapes of the domains is critical for NHE1 binding orientation.

Notably the shape of the interaction surfaces of NHE1-CHP1 and CNA-CNB differs. The spatial arrangement of NHE1 and CNA residues that contribute to form the interaction surfaces differs for each (Fig. 6*B*). Only Val-349, Phe-350, and Val-357 of CNA are located at equivalent positions to Ile-522, His-523, and Leu-530 of NHE1 unlike other residues. Cleary Trp-352 and Phe-356 of CNA that interact with the roof of the hydrophobic cleft formed by CNB are missing in NHE1. Furthermore the interactions mediated by the C-terminal stretch region of CNA, where Leu-369 and Leu-371 protrude, are absent in NHE1. On the other hand, the corresponding residues to Phe-526 and Ile-518 of NHE1 are absent in CNA.

Consequently the interaction mechanism dominated by hydrophobic interactions through amphipathic helices and four EF-hands is common in both complexes, but their shape differs. This surface complementarity in terms of a knobs-into-hole mode of interaction defines the binding specificity of these proteins, although the folding topology is identical.

Correlation with Mutagenesis Studies—The solution structure of the CHP1-NHE1 complex is essentially consistent with previous mutagenesis studies concerning NHE1. Co-immunoprecipitation experiments showed that the 4Q mutant of NHE1, in which Phe-526, Leu-527, Leu-530, and Leu-531 are substituted with glutamine, displayed no binding to CHP1, whereas the I518Q/I522Q NHE1 double mutant displayed some binding albeit with decreased affinity (3). Our structure determination revealed that Phe-526, Leu-527, Leu-530, and Leu-531 form a hydrophobic core that interacts with the center of the hydrophobic cleft of the C-terminal domain of

CHP1, whereas Ile-518 and Ile-522 interact with the rim of the hydrophobic cleft of the C-terminal domain of CHP1 (Figs. 4*B* and 6*A*). Deletion mutagenesis indicated that NHE1 (residues 510–575) retained binding affinity similar to the wild-type protein, implying that the juxtamembrane region of NHE1 comprising residues 503–509 is unimportant for CHP1 binding (3). These residues were found to be unstructured in the present study and form no direct contact with NHE1.

The binding activity of NHE1 (residues 530–656) lacking the N-terminal segment was found to be completely impaired (3). Our NHE1-CHP1 complex structure shows that an absence of residues preceding Leu-530 results in almost complete loss of interaction between NHE1 and the C-terminal domain of CHP1, whereas the many hydrophobic interactions mediated by NHE1 residues Leu-530, Leu-531, Ile-534, and Ile-537 are retained (Fig. 6*A*). This indicates that interaction of the N-terminal residues of NHE1 and the C-terminal domain of CHP1 is indispensable in maintaining the NHE1-CHP1 complex. Namely this part of the interaction plays a dominant role in NHE1-CHP1 complex formation.

CHP1 was subjected to site-directed mutagenesis in an effort to reveal detailed individual contributions of interfacial residues toward the overall stability of the NHE1-CHP1 complex. We selected three categories of residues in CHP1: 1) residues that comprise the floor of the hydrophobic pocket, Phe-70, Phe-90, Phe-117, Ala-118, Leu-121, Tyr-122, and Met-189; 2) residues forming the rim of the pocket, Ile-66, Leu-139, Met-142, and Val-185; and 3) a residue forming the salt bridge, Lys-188. A noninteracting solvent-exposed residue, Val-102, as the positive control and a triple mutation involving hydrophobic residues Phe-90/Leu-87/Leu-54 and Phe-176/Met-142/Tyr-122 as the negative control were prepared.

Dramatic effects were observed in terms of CHP1 binding to NHE1 with mutations F117Q, Y122Q, and V185Q (Fig. 6*C*). We expected the floor-forming residues located at the bottom of the cleft to be critical for the interaction, but the rim-forming residue Val-185 showed significant reduction similar to the negative control. Based on the solution structure of the NHE1-CHP1 complex, it was appeared that Phe-117, Tyr-122, and Val-185 were confined to the C-terminal domain of CHP1 and were packed against the apolar side of NHE1. This suggests that the C-terminal hydrophobic cleft represents a mutation hot spot, implying that it plays a key role in the NHE1-CHP1 interaction. This result is consistent with the NHE1 deletion result indicating that interaction between the N-terminal segment of NHE1 and the C-terminal domain of CHP1 is dominant. This represents a unique feature of the NHE1-CHP1 interaction.

Although mutation of residues possibly involved in salt bridge formation such as K188E and K188R resulted in a marked decrease in binding interaction, the effect was not strong, and the charge-reversing effect of K188E was unclear. Thus, it appears that although this salt bridge contributes to NHE1-CHP1 complex formation, it is not the main force possibly because this bond is exposed to solvent (Fig. 6*A*), and therefore solvation could weaken the strength of the interaction.

Role of CHP1—NMR investigations of NHE1 complexed with CHP1 revealed that the juxtamembrane region comprising residues 503–517 was unstructured in solution. This region is rich in basic residues with a previous study reporting that NHE1 comprising residues 506–576 bound to PIP_2 *in vitro* (13). In addition, residues 513–520 and 556–564 might represent PIP_2 binding sites (13). Accordingly it is likely that this juxtamembrane region (residues 503–517) following the last transmembrane helix (H12, residues 478–499) is incapable of forming a continuous straight helical structure into the cytoplasm due to interaction with the membrane. Rather the overall structure of NHE1 presumably turns or bends toward the cytoplasmic membrane following a PIP_2-mediated interaction. Assuming that flanking regions of the helix, residues 513–520 and 556–564, attach to the membrane (PIP_2) (13), the helix and CHP1 should be located immediately beneath the cytoplasmic membrane.

Furthermore it has been reported that NHE1 acts as a scaffold protein linked to actin filaments via ezrin-radixin-moesin proteins in addition to possessing function as an ion exchanger (52, 53). Our NMR studies revealed that the cytoplasmic helix-forming residues of NHE1 comprise residues 518–537, which showed little overlap from the previously reported ezrin-radixin-moesin binding region (512–520 and 550–565). This ensures simultaneous binding of NHE1 to CHP1 and ezrin-radixin-moesin proteins.

The juxtamembrane region of NHE1 forms a particular tertiary or quaternary structure that is mediated by interactions with the membrane (PIP_2), CHP1, and ezrin-radixin-moesin proteins. The overall structure of the juxtamembrane region might play an important role in NHE1 activity. The 90% loss in activity following CHP1 depletion might be due to disruption of the structure of the cytoplasmic region of NHE1 around the membrane. In fact, although this represents *in vitro* evidence, the amphipathic helix is disrupted in the absence of CHP1 based on the CD and NMR data (supporting information S2 and S3).

Possible Mode of Regulation—CHP1 deprivation resulted in impaired regulation of NHE1 following external stimuli, implying that CHP1 acts as regulator of NHE1 by involvement in the processing of intracellular signals derived from external stimuli. However, the regulatory mechanism remains unclear. Although it was reported that CHP1 is an *N*-myristoylated protein, CHP1 does not exert myristoyl switching in a Ca^{2+}-dependent manner under normal physiological conditions because EF-3 and EF-4 constitutively bind Ca^{2+} ions where *N*-myristoylation was not required for NHE1 binding, activation, or localization (14).

Of particular note, it was reported that CHP1 is a phosphorylated protein, although the phosphorylation sites were not determined. According to the phosphorylation prediction server NetPhos (54), the CHP1 sequence contains potential phosphorylation sites located at residues Thr-36, Ser-37, Ser-47, Ser-131, and Ser-172 (score, >0.8). Similarly the phosphorylation server Scansite (55) identified potential phosphorylation sites located at residues Thr-36, Ser-37, and Ser-172 (score, >0.5). From the determined NHE1-CHP1 structure, residues Thr-36, Ser-37, and Ser-172, predicted by both servers as potential phosphorylation sites, are locate at the terminal part of the EF-hand helix or its flanking loop where the side chains of

the aforementioned residues are exposed to the protein surface reinforcing the possibility of phosphorylation. Phosphorylation-induced conformational changes in CHP1 and the subsequent regulation of NHE1 activity are interesting areas that remain to be investigated.

Conclusion—We have determined the solution structure of the cytoplasmic region of NHE1 complexed with CHP1. Although previous biochemical analyses suggested that the hydrophobic residues of NHE1 were likely to interact with CHP1, the present study has delineated the structural basis for this interaction. The solution structure provides concrete evidence that the cytoplasmic region of NHE1 forms an amphipathic helix that interacts directly with the large concave undersurface of CHP1. This helix is disrupted in the absence of CHP1; thus the loss in activity following CHP1 depletion might be due to disruption of the structure of the juxtamembrane region of NHE1. Our structure provides a first step toward understanding the regulation of NHE1 activity. Moreover it revealed a novel target binding mechanism mediated by four EF-hands. These findings should facilitate future studies aimed at understanding the mechanism underlying recognition utilized by EF-hand proteins that are engaged in signal transduction pathways and many other molecular and cellular events. During the initial review of our manuscript, a study appeared that describes a crystal structure of the NHE1 peptide complexed with CHP2 containing Y^{3+} ions instead of Ca^{2+} (56).

Acknowledgments—We are grateful to Momoko Yoneyama, Hiroko Kinoshita, and Junko Tsukamoto of the Nara Institute of Science and Technology for technical assistance and Kokoro Hayashi for help in sample preparation.

REFERENCES

1. Orlowski, J., and Grinstein, S. (2004) *Pfluegers Arch. Eur. J. Physiol.* **447,** 549–565
2. Lin, X., and Barber, D. L. (1996) *Proc. Natl. Acad. Sci. U. S. A.* **93,** 12631–12636
3. Pang, T., Su, X., Wakabayashi, S., and Shigekawa, M. (2001) *J. Biol. Chem.* **276,** 17367–17372
4. Bertrand, B., Wakabayashi, S., Ikeda, T., Pouyssegur, J., and Shigekawa, M. (1994) *J. Biol. Chem.* **269,** 13703–13709
5. Wakabayashi, S., Bertrand, B., Ikeda, T., Pouyssegur, J., and Shigekawa M. (1994) *J. Biol. Chem.* **269,** 13710–13715
6. Dhanasekaran, N., Prasad, M. V., Wadsworth, S. J., Dermott, J. M., and van Rossum, G. (1994) *J. Biol. Chem.* **269,** 11802–11806
7. Hooley, R., Yu, C. Y., Symons, M., and Barber, D. L. (1996) *J. Biol. Chem.* **271,** 6152–6158
8. Voyno-Yasenetskaya, T., Conklin, B. R., Gilbert, R. L., Hooley, R., Bourne, H. R., and Barber, D. L. (1994) *J. Biol. Chem.* **269,** 4721–4724
9. Bianchini, L., L'Allemain, G., and Pouyssegur, J. (1997) *J. Biol. Chem.* **272,** 271–279
10. Takahashi, E., Abe, J., Gallis, B., Aebersold, R., Spring, D. J., Krebs, E. G., and Berk, B. C. (1999) *J. Biol. Chem.* **274,** 20206–20214
11. Lehoux, S., Abe, J.-i., Florian, J. A., and Berk, B. C. (2001) *J. Biol. Chem.* **276,** 15794–15800
12. Yan, W., Nehrke, K., Choi, J., and Barber, D. L. (2001) *J. Biol. Chem.* **276,** 31349–31356
13. Aharonovitz, O., Zaun, H. C., Balla, T., York, J. D., Orlowski, J., and Grinstein, S. (2000) *J. Cell Biol.* **150,** 213–224
14. Pang, T., Hisamitsu, T., Mori, H., Shigekawa, M., and Wakabayashi, S. (2004) *Biochemistry* **43,** 3628–3636
15. Barroso, M. R., Bernd, K. K., DeWitt, N. D., Chang, A., Mills, K., and Sztul, E. S. (1996) *J. Biol. Chem.* **271,** 10183–10187
16. Lin, X., Sikkink, R. A., Rusnak, F., and Barber, D. L. (1999) *J. Biol. Chem.* **274,** 36125–36131
17. Timm, S., Titus, B., Bernd, K., and Barroso, M. (1999) *Mol. Biol. Cell* **10,** 3473–3488
18. Matsumoto, M., Miyake, Y., Nagita, M., Inoue, H., Shitakubo, D., Takemoto, K., Ohtsuka, C., Murakami, H., Nakamura, N., and Kanazawa, H. (2001) *J. Biochem. (Tokyo)* **130,** 217–225
19. Nakamura, N., Miyake, Y., Matsushita, M., Tanaka, S., Inoue, H., and Kanazawa, H. (2002) *J. Biochem. (Tokyo)* **132,** 483–491
20. Pang, T., Wakabayashi, S., and Shigekawa, M. (2002) *J. Biol. Chem.* **277,** 43771–43777
21. Mailander, J., Muller-Esterl, W., and Dedio, J. (2001) *FEBS Lett.* **507,** 331–335
22. Perera, E. M., Martin, H., Seeherunvong, T., Kos, L., Hughes, I. A., Hawkins, J. R., and Berkovitz, G. D. (2001) *Endocrinology* **142,** 455–463
23. Naoe, Y., Arita, K., Hashimoto, H., Kanazawa, H., Sato, M., and Shimizu, T. (2005) *J. Biol. Chem.* **280,** 32372–32378
24. Yamazaki, T., Lee, W., Arrowsmith, C. H., Muhandiram, D. R., and Kay, L. E. (1994) *J. Am. Chem. Soc.* **116,** 11655–11666
25. Matsuo, H., Kupce, E., Li, H., and Wagner, G. (1996) *J. Magn. Reson. B* **111,** 194–198
26. Muhandiram, D. R., and Kay, L. E. (1994) *J. Magn. Reson. B* **103,** 203–216
27. Clowes, R. T., Boucher, W., Hardman, C. H., Domaille, P. J., and Laue, E. D. (1993) *J. Biomol. NMR* **3,** 349–354
28. Kay, L. E., Xu, G. Y., Singer, A. U., Muhandiram, D. R., and Formankay, J. D. (1993) *J. Magn. Reson. B* **101,** 333–337
29. Logan, T. M., Olejniczak, E. T., Xu, R. X., and Fesik, S. W. (1993) *J. Biomol. NMR* **3,** 225–231
30. Neri, D., Szyperski, T., Otting, G., Senn, H., and Wuthrich, K. (1989) *Biochemistry* **28,** 7510–7516
31. Boucher, W., Laue, E. D., Campbell-Burk, S., and Domaille, P. J. (1992) *J. Am. Chem. Soc.* **114,** 2262–2264
32. Cavanagh, J., Fairbrother, W. J., Palmer, A. G., III, and Skelton, N. J. (1996) *Protein NMR Spectroscopy*, pp. 301–531, Academic Press, San Diego, CA
33. Grzesiek, S., and Bax, A. (1993) *J. Biomol. NMR* **3,** 185–204
34. Delaglio, F., Grzesiek, S., Vuister, G. W., Zhu, G., Pfeifer, J., and Bax, A. (1995) *J. Biomol. NMR* **6,** 277–279
35. Goddard, T. D., and Kneller, D. G. (1999) *SPARKY3*, University of California, San Francisco
36. Herrmann, T., Guntert, P., and Wuthrich, K. (2002) *J. Mol. Biol.* **319,** 209–227
37. Schwieters, C. D., Kuszewski, J. J., Tjandra, N., and Clore, G. M. (2003) *J. Magn. Reson.* **160,** 65–73
38. Laskowski, R. A., Rullmannn, J. A., MacArthur, M. W., Kaptein, R., and Thornton, J. M. (1996) *J. Biomol. NMR* **8,** 477–486
39. Koradi, R., Billete, M., and Wuthrich, K. (1996) *J. Mol. Graph.* **14,** 51–55
40. Nicholls, A., Sharp, K. A., and Honig, B. (1991) *Proteins Struct. Funct. Genet.* **11,** 281–296
41. Pettersen, E. F., Goddard, T. D., Huang, C. C., Couch, G. S., Greenblatt, D. M., Meng, E. C., and Ferrin, T. E. (2004) *J. Comput. Chem.* **25,** 1605–1612
42. Goda, N., Tenno, T., Takasu, H., Hiroaki, H., and Shirakawa, M. (2004) *Protein Sci.* **13,** 652–658
43. Hoeflich, K. P., and Ikura, M. (2002) *Cell* **108,** 739–742
44. Bhattacharya, S., Bunick, C. G., and Chazin, W. J. (2004) *Biochim. Biophys. Acta* **1742,** 69–79
45. Zhou, W., Qian, Y., Kunjilwar, K., Pfaffinger, P. J., and Choe, S. (2004) *Neuron* **41,** 573–586
46. Griffith, J. P., Kim, J. L., Kim, E. E., Sintchak, M. D., Thomson, J. A., Fitzgibbon, M. J., Fleming, M. A., Caron, P. R., Hsiao, K., and Navia, M. A. (1995) *Cell* **82,** 507–522
47. Kissinger, C. R., Parge, H. E., Knighton, D. R., Lewis, C. T., Pelletier, L. A., Tempczyk, A., Kalish, V. J., Tucker, K. D., Showalter, R. E., Moomaw, E. W., Gastinel, L. N., Habuka, N., Chen, X., Maldonado, F., Barker, J. E., Bacquet, R., and Villafranca, J. E. (1995) *Nature* **378,** 641–644
48. Yap, K. L., Ames, J. B., Swindells, M. B., and Ikura, M. (1999) *Proteins* **37,**

499–507
49. Yap, K. L., Ames, J. B., Swindells, M. B., and Ikura, M. (2002) *Methods Mol. Biol.* **173,** 317–324
50. Burgoyne, R. D., and Weiss, J. L. (2001) *Biochem. J.* **353,** 1–12
51. Salerno, W. J., Seaver, S. M., Armstrong, B. R., and Radhakrishnan, I. (2004) *Nucleic Acids Res.* **32,** W566–W568
52. Baumgartner, M., Patel, H., and Barber, D. L. (2004) *Am. J. Physiol.* **287,** C844–C850
53. Denker, S. P., Huang, D. C., Orlowski, J., Furthmayr, H., and Barber, D. L. (2000) *Mol. Cell* **6,** 1425–1436
54. Blom, N., Gammeltoft, S., and Brunak, S. (1999) *J. Mol. Biol.* **294,** 1351–1362
55. Obenauer, J. C., Cantley, L. C., and Yaffe, M. B. (2003) *Nucleic Acids Res.* **31,** 3635–3641
56. Ammar, Y. B., Takeda, S., Hisamitsu, T., Mori, H., and Wakabayashi, S. (2006) *EMBO J.* **25,** 2315–2325

THE JOURNAL OF BIOLOGICAL CHEMISTRY VOL. 282, NO. 4, pp. 2741–2751, January 26, 2007

Solution Structure of the Cytoplasmic Region of Na^+/H^+ Exchanger 1 Complexed with Essential Cofactor Calcineurin B Homologous Protein 1*[S]

Received for publication, April 28, 2006, and in revised form, October 6, 2006 Published, JBC Papers in Press, October 18, 2006, DOI 10.1074/jbc.M604092200

Masaki Mishima[‡], Shigeo Wakabayashi[§], and Chojiro Kojima[‡1]

From the [‡]Graduate School of Biological Sciences, Nara Institute of Science and Technology, Ikoma, Nara 630-0192, Japan and [§]Department of Molecular Physiology, National Cardiovascular Center Research Institute, Suita, Osaka 565-8565, Japan

Na^+/H^+ exchanger 1 (NHE1) regulates intracellular pH, Na^+ content, and cell volume. Calcineurin B homologous protein 1 (CHP1) serves as an essential cofactor that facilitates NHE1 exchange activity under physiological conditions by direct binding to the cytoplasmic juxtamembrane region of NHE1. Here we describe the solution structure of the cytoplasmic juxtamembrane region of NHE1 complexed with CHP1. The region of NHE1 forms an amphipathic helix, which is induced by CHP1 binding, and CHP1 possesses a large hydrophobic cleft formed by EF-hand helices. The apolar side of the NHE1 helix participates in extensive hydrophobic interactions with the cleft of CHP1. We suggest that helix formation of the cytoplasmic region of NHE1 by CHP1 is a prerequisite for generating the active form of NHE1. The molecular recognition detailed in this study also provides novel insight into the target binding mechanism of EF-hand proteins.

Na^+/H^+ exchangers comprise a family of countertransport proteins that catalyze the electroneutral exchange of Na^+ and H^+. Nine isoforms of the Na^+/H^+ exchanger have been isolated and shown to possess similar membrane topologies consisting of 12 N-terminal membrane-spanning helices and a large C-terminal cytoplasmic region (Fig. 1*A*). The exchanger isoforms exhibit tissue-specific expression, membrane localization, and kinetic and pharmacological properties (1). They participate in a broad range of physiological processes including the regulation of cell volume, transepithelial transport of electrolytes, cell proliferation, apoptosis, and differentiation. Isoforms NHE1–5, localized at the plasma membrane, are primarily involved in the regulation of intracellular pH (pH_i)[2] and Na^+ concentration (1).

Of them, the ubiquitously expressed isoform NHE1 is the best studied mammalian Na^+/H^+ exchanger. The activity is controlled by various extrinsic factors including hormones, growth factors, pharmacological agents, and mechanical stimuli (1). The regulation of NHE1 by these external stimuli is thought to be exerted through the action of a variety of signaling molecules including calcineurin B homologous protein (2, 3), calmodulin (4, 5), low molecular mass GTPases of the Ras and Rho family (6–8), p42/44 mitogen-activated protein kinases (9), p90 ribosomal S6 kinase (10), 14-3-3 protein (11), Nck-interacting kinase (12), and phosphatidylinositol 4,5-bisphosphate (13). However, the detailed mechanism through which these events occur remains unknown.

Among these factors, CHP1 can serve as an essential cofactor and is required by at least three NHE isoforms (NHE1–3) to express high physiological levels of exchange activity (3). It was shown that CHP1 bound directly to the juxtamembrane region of the C-terminal cytoplasmic domain. When GFP-CHP1 and NHE1–3 were co-expressed, it was found that GFP-CHP1 was mostly localized at the cell surface, whereas co-expression of CHP1 and a CHP1 binding-defective NHE1 mutant failed to show co-localization, implying that NHE1 is a principal target of CHP1 (3). In addition to reduced activity in the neutral pH range, the CHP1 binding-defective NHE1 mutant showed a marked reduction in pH_i sensitivity (~0.7 pH unit acidic shift) that subsequently abolished various NHE1 regulatory responses. Furthermore CHP1 deprivation resulted in marked reduction (>90%) of NHE1 activity (3). These observations suggest that the association of NHE1 with CHP1 is critical for activity and the maintenance of NHE1 pH_i sensitivity (14).

CHP1 consists of four EF-hands, the primary sequence of which is homologous to calmodulin (CaM) and calcineurin B

* This work was supported in part by grants-in-aid for Scientific Research on Priority Area and the 21st Century of Excellence (COE) Program from the Ministry of Education, Culture, Sports, Science and Technology (MEXT), Japan (to M. M. and C. K.), and Grant nano-001 for Research on Advanced Medical Technology from the Ministry of Health, Labor and Welfare of Japan and Grant-in-aid for Priority Areas 13142210 for Scientific Research from the MEXT (to S. W.). The costs of publication of this article were defrayed in part by the payment of page charges. This article must therefore be hereby marked "*advertisement*" in accordance with 18 U.S.C. Section 1734 solely to indicate this fact.

[S] The on-line version of this article (available at http://www.jbc.org) contains supplemental Table S1 and Figs. S2 and S3.

The atomic coordinates and structure factors (code 2E30) have been deposited in the Protein Data Bank, Research Collaboratory for Structural Bioinformatics, Rutgers University, New Brunswick, NJ (http://www.rcsb.org/).

[1] To whom correspondence should be addressed: Graduate School of Biological Sciences, Nara Institute of Science and Technology, 8916-5 Takayama, Ikoma, Nara 630-0192, Japan. Tel.: 81-743-72-5571; Fax: 81-743-72-5579; E-mail: kojima@bs.naist.jp.

[2] The abbreviations used are: pH_i, intracellular pH; HSQC, heteronuclear single quantum coherence; NOE, nuclear Overhauser effect; NOESY, NOE spectroscopy; TOCSY, total correlation spectroscopy; CANDID, combined automated NOE assignment and structure determination module; CaM, calmodulin; CNB, calcineurin B; NHE, Na^+/H^+ exchanger; CHP, calcineurin B homologous protein; CNA, calcineurin A; Ni-NTA, nickel-nitrilotriacetic acid; GST, glutathione *S*-transferase; CHAPS, 3-[(3-cholamidopropyl)dimethylammonio]-1-propanesulfonic acid; r.m.s., root mean square; Kv, voltage-gated potassium channel; KChIP, Kv-interacting protein; PIP_2, phosphatidylinositol 4,5-bisphosphate.

Supplemental Material can be found at: http://www.jbc.org/cgi/content/full/M604092200/DC1

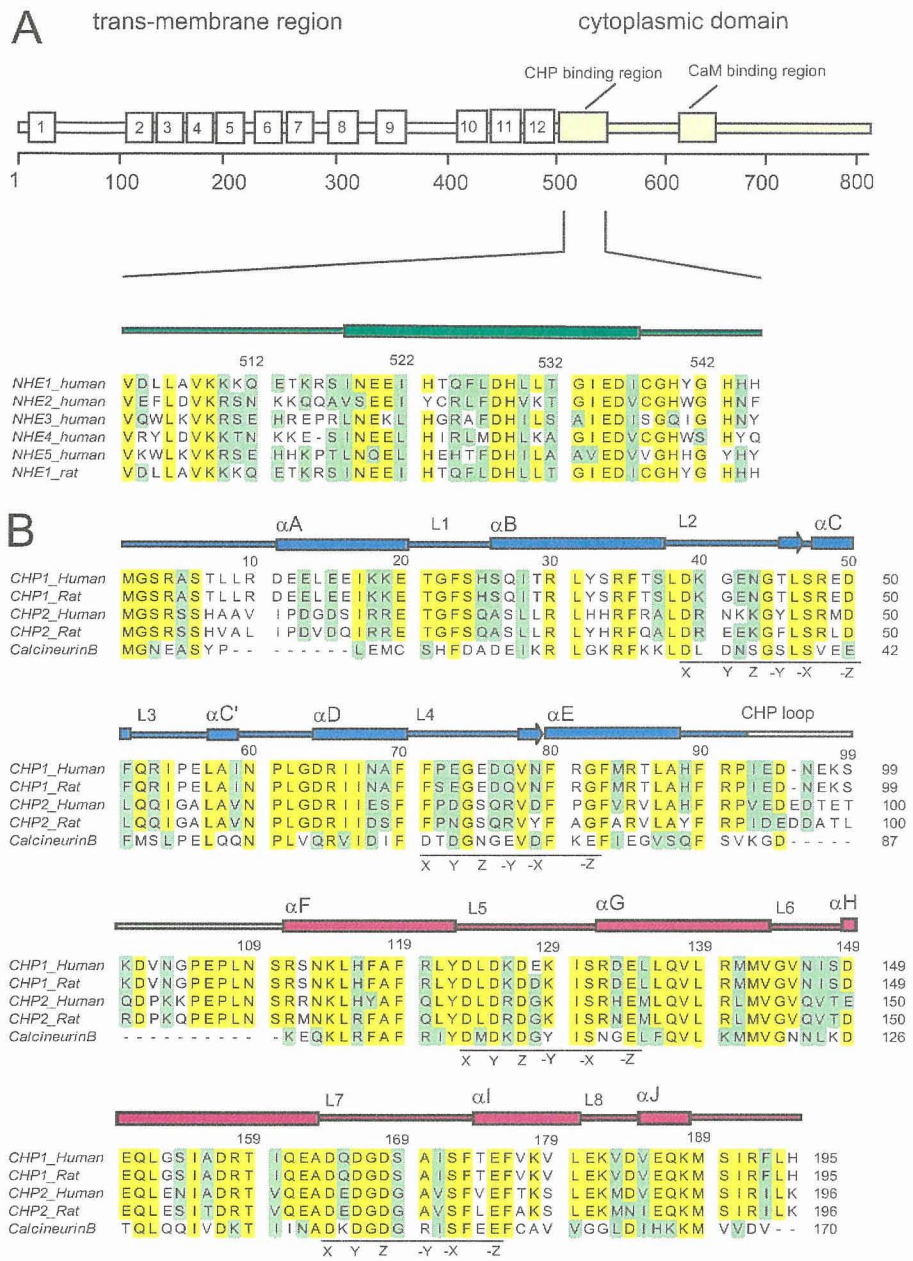

FIGURE 1. **Multiple sequence alignments of NHE1 and CHP1.** *A*, domain structure and alignment of NHE1. *B*, alignment of CHP1, CHP2, and human calcineurin B. In *A* and *B*, sequence alignment was performed using ClustalW. Secondary structure elements of the proteins are shown schematically at the *top* of the alignments. N- and C-terminal domains of CHP1 are colored in *blue* and *magenta*, respectively, for clarity. Conserved and semiconserved residues are colored in *yellow* and *green*, respectively. The 12-residue motif involved in the EF-hand is *underlined*, and key residues are indicated as *X*, *Y*, *Z*, *-Y*, *-X*, and *-Z*.

(CNB), possessing 31 and 41% sequence identity, respectively (Fig. 1*B*). It is well known that all CaM and CNB EF-hands can bind Ca^{2+}. However, CHP1 EF-1 and EF-2 are ancestral and do not bind Ca^{2+} under physiological conditions, whereas EF-3 and EF-4 bind two Ca^{2+} ions with high affinity (~90 nM) based on the $^{45}Ca^{2+}$ binding experiments for several CHP1 mutants (14). Complex formation between CHP1 and the CHP1 binding domain of NHE1 resulted in a marked increase in Ca^{2+} binding affinity (K_d = ~2 nM) (14). This suggests that CHP1 constitutively contains two Ca^{2+} ions when associated with NHE1 in cells (14).

Interestingly CHP1 has been reported to exhibit multiple functions. It was initially identified as a protein (p22) involved in vesicular transport (15) and the inhibition of calcineurin phosphatase activity (16). It was also found to interact with microtubules (17), DRAK2 (death-associated protein kinase-related apoptosis-inducing protein kinase 2) (18) and KIF1Bβ2 (kinesin family 1Bβ2) (19).

A second CHP isoform, CHP2, with 61% sequence identity was also identified and found to be involved in the maintenance of abnormally high pH_i in malignantly transformed cells. CHP2 is expressed at a relatively high level in malignantly transformed cells and in rat small intestine, suggesting that it plays a specific role in this tissue (20). In addition, tescalcin, an EF-hand protein closely related to CNB, that interacts with the cytoplasmic region of NHE1 has been identified (21, 22).

The crystal structure of NHE1-unbound rat CHP1 was recently determined and revealed that the overall structure is similar to CNB where Ca^{2+} ions are coordinated within EF-3 and EF-4. However, the interaction mechanism between NHE1 and CHP1 remains unknown (23).

Here we report on the solution structure of the cytoplasmic region of NHE1 bound to CHP1 as determined by NMR. Details of the NHE1-CHP1 interaction are described. We present mutational binding data to delineate the significance of the interactions observed in the complex. Based on the structure, we suggest a role for CHP1 in terms of NHE1 activation. Comparisons of the binding mode between NHE1-CHP1 and calcineurin A (CNA), CNB, and other related four-EF-hand proteins are also discussed.

EXPERIMENTAL PROCEDURES

Sample Preparation—The NHE1-CHP1 complex was co-expressed and co-purified. DNA encoding NHE1 was cloned into the pET24a vector (Novagen), and CHP1 was subcloned into pET11a (Novagen), which produces recombinant protein with a hexahistidine (His_6) sequence at the C terminus. The proteins were co-overexpressed in *Escherichia coli* BL21(DE3) cells. Uniformly ^{15}N- and $^{15}N/^{13}C$-labeled proteins were prepared by

growing bacteria in minimal medium containing $^{15}NH_4Cl$ with or without [$^{13}C_6$]glucose. Uniformly $^{15}N/^{13}C$-labeled and fractionally deuterated protein sample was prepared using medium containing 60% ^2H_2O. The NHE1-CHP1 complex was purified using a standard Ni-NTA affinity column protocol (Qiagen). Further purification was performed by gel filtration using Superdex 200 (GE Healthcare). NMR samples contained 0.5–0.9 mM protein in 50 mM Tris-d_7 buffer (pH 6.9), 1 mM dithiothreitol-d_{10}, 30 mM KCl in $H_2O/^2H_2O$ (9:1) or ^2H_2O.

NMR Spectroscopy—NMR data were recorded at 37 °C on Bruker AVANCE 500 and DRX 800 NMR spectrometers. Resonance assignments for ^{1}HN, ^{15}N, $^{13}C\alpha$, $^{13}C\beta$, and $^{13}C'$ nuclei for the CHP1-NHE1 complex were obtained through the following ^{2}H-decoupled, triple resonance spectra applied to a fractionally deuterated $^{15}N/^{13}C$-labeled sample: three-dimensional HNCACB/HN(CO)CACB (24) and three-dimensional HN(CA)CO/HNCO experiments (25, 26). Side-chain ^{1}H and ^{13}C resonances were assigned on a fully protonated sample or a fractionally deuterated $^{15}N/^{13}C$-labeled sample using three-dimensional C(CO)NH, three-dimensional H(CCO)NH, four-dimensional HC(CO)NH, and three-dimensional HCCH TOCSY (27–29). Stereospecific assignment of leucine and valine methyl groups were obtained from a Constant Time-$^1H/^{13}C$ HSQC spectrum of a 15% ^{13}C-labeled sample (30). $^1H\alpha$ and $^1H\beta$ resonance assignments were supplemented with three-dimensional H(CACO)NH (31), ^{15}N-edited TOCSY-HSQC (32), and three-dimensional HBHA(CBCACO)NH (33). Aromatic resonances of both NHE1 and CHP1 were mainly assigned using three-dimensional ^{13}C-aromatic-edited/^{15}N-separated NOESY-HSQC, three-dimensional ^{13}C-edited NOESY, ^1H-^1H TOCSY, and NOESY experiments (32). The assignment was verified using the Constant Time-$^1H/^{13}C$ HSQC spectrum of a 15% ^{13}C-labeled sample (30). The following NOESY spectra were recorded for the protonated sample and used to generate distance restraints for structure calculations: three-dimensional ^{15}N-edited NOESY (80-ms mixing time), three-dimensional ^{13}C-edited NOESY (80-ms mixing time), and two-dimensional ^{1}H NOESY (80-ms mixing time). Slowly exchanging amide protons were identified from a series of two-dimensional ^{15}N HSQC spectra recorded after the H_2O buffer was replaced with ^2H_2O buffer. All NMR spectra were processed using NMRPipe/NMRDraw (34) analyzed using SPARKY (35).

Structure Calculations—Intramolecular and intermolecular distance constraints were identified in the three-dimensional $^{15}N/^{13}C$-separated NOESY spectra using a $^{15}N/^{13}C$-labeled NHE1-CHP sample with mixing times of 80 ms. Backbone hydrogen bond restraints within regular secondary structure elements that were consistent with backbone amide hydrogen/deuterium exchange data were included in the structure calculations. The initial structure calculations were performed by iterative automated assignment of the NOE spectra using CANDID (36) in addition to manually assigned NOE-derived distance restraints. The restraints, leading to converged structures, were subsequently utilized for the iterative automated assignment of all spectra including aromatic residues using CANDID. Finally refinement of the structures (including two Ca^{2+} ions) using XPLOR-NIH (version 2.96) was performed (37). The final structure calculations used a total of 4022 NOE-derived distance restraints obtained from the manual and the CANDID-assisted assignments from the ^{15}N- or ^{13}C-edited NOE data. A total of 100 simulated annealing structures were calculated, and 20 structures were selected that possessed no NOE violations greater than 0.5 Å and no dihedral violations greater than 5°. Final structures were evaluated using the program ProcheckNMR (38). Structures and figures were drawn using MOLMOL (39), GRASP (40), and Chimera (41).

Mutagenesis and GST Pulldown Assay—For the binding analyses, CHP1 was expressed as a fusion protein with GST in *E. coli*, which was then subcloned into modified pGEX6P-3 (Novagen) (42). Site-directed mutant proteins were prepared using the QuikChange kit (Stratagene). DNA sequencing confirmed the mutations. Vectors were transformed into BL21(DE3)star (Invitrogen). Cells were grown at 37 °C and then induced with 1 mM isopropyl 1-thio-β-D-galactopyranoside for 12 h at 20 °C. Harvested cells were disrupted via sonication in HEPES (pH 8.0) containing 10% glycerol, 10% sucrose, 1 mM dithiothreitol, and 30 mM KCl. The GST-CHP1 fusion protein was purified using glutathione-Sepharose (GE Healthcare) and a standard protocol except that the equilibrium buffer was changed to 50 mM HEPES buffer (pH 8.0) containing 10% glycerol, 1 mM dithiothreitol, and 30 mM KCl, and the column was washed extensively with 20 mM CHAPS. The effect of mutation on the binding of CHP1 to NHE1 peptides was characterized using a GST pulldown assay. Synthetic NHE1 peptide (residues 514–545 including a hexahistidine sequence at the C terminus) was purchased from Greiner Japan (Tokyo, Japan). Briefly wild-type and CHP1 mutant GST fusion proteins, in addition to GST alone, were incubated for 30 min at 20 °C with NHE1 peptide in binding buffer containing 50 mM HEPES (pH 7.5), 20 mM CHAPS, 10% glycerol, 1 mM Pefabloc, and 1 mM dithiothreitol. GST protein-bound Sepharose beads were washed extensively with binding buffer. Proteins were resolved by 12% NuPAGE (Invitrogen) and blotted onto membranes, and then His-NHE1 was analyzed with Ni-NTA-conjugated alkaline phosphatase (Promega) and Western Blue substrate (Promega). Quantification was represented as the average value of experiments performed in triplicate.

RESULTS AND DISCUSSION

Structure Determination—To better understand the mechanism pertaining to CHP1-regulated NHE1 activity, the solution structure of unmyristoylated CHP1 complexed with the cytoplasmic region (503–545) of NHE1 was determined by NMR spectroscopy. Our structural studies were initially hampered by the fact that NHE1-free CHP1 tended to aggregate during NMR measurements, and the CHP1-unbound cytoplasmic region (503–545) of NHE1 readily degraded during the expression and purification steps. Consequently NMR structural analysis of co-expressed and co-purified samples was undertaken. Co-expression of CHP1 and NHE1-(503–545) produced a stable complex for structural studies and showed no significant degradation and aggregation for several weeks.

The ^1H-^{15}N HSQC spectrum of NHE1-unbound CHP1 displays many broadened peaks presumably due to formation of a dimer, multimer, or an equilibrium between these states in solution. In contrast, the HSQC spectrum of ^{15}N-labeled CHP1

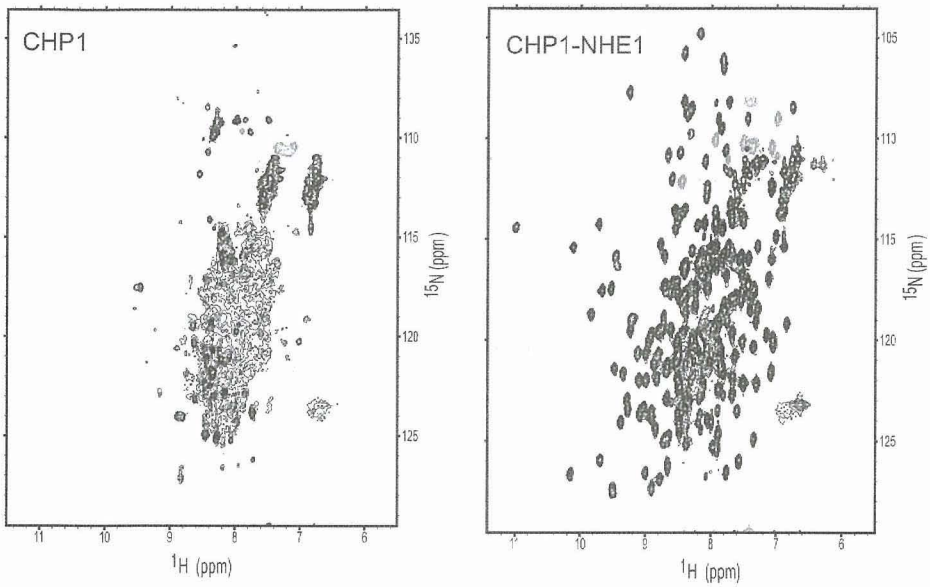

FIGURE 2. **^{1}H-^{15}N HSQC spectra of ^{1}5N-labeled NHE1-free CHP1 (*left image*) and ^{15}N-labeled NHE1-(503–545)-CHP1 complex (*right image*).** These spectra were obtained with 0.3 mM samples at pH 6.9 and 37 °C recorded on the AVANCE 500.

TABLE 1

Structural statistics for NHE1-CHP1

These statistics represent an ensemble comprising 20 of the lowest energy structures obtained from 150 starting structures. Structure calculations were performed using XPLOR-NIH version 2.9.6.

Total number of distance constraints	4242
Long range ($\|i-j\|>4$)	589 (inter: 134)
Middle range ($\|i-j=2, 3, 4$)	874
Short range ($\|i-j\|=1$)	1038
Intraresidue	1521
Hydrogen bond constraints (including Ca^{2-} coordination restraints)	110 × 2
Dihedral constraints	
ϕ, φ	105, 105
$\chi 1$	17
r.m.s. deviation from experimental constraints[a]	
Distance (Å)	$0.0288 \pm 7 \times 10^{-4}$
Angle (°)	$0.44 \pm 3 \times 10^{-2}$
r.m.s. deviation from idealized covalent geometry	
Bonds (Å)	$0.00248 \pm 6 \times 10^{-5}$
Angles (°)	$0.360 \pm 6 \times 10^{-3}$
Impropers (°)	$0.31 \pm 1 \times 10^{-2}$
XPLOR energy terms (kcal/mol)[b]	
E_{bond}	23 ± 1
E_{angle}	138 ± 5
E_{imp}	28 ± 2
$E_{vdw(LJ)}$	$-6.6 \times 10^{2} \pm 0.2 \times 10^{2}$
PROCHECK Ramachandran plot (185–254)	
Residues in most favored regions (%)	78.6
Residues in additional allowed regions (%)	18.1
Residues in generously allowed regions (%)	2.9
Residues in disallowed regions (%)	0.4
r.m.s. deviation of mean structure derived from 30 calculated structures	
Backbone (10–92, 108–192, 516–538) (Å)	0.53
All heavy (10–92, 108–192, 516–538) (Å)	1.15

[a] None of these structures exhibited distance violations >0.5 or dihedral angle violations >5°.

[b] $E_{vdw(LJ)}$ represents the Lennard-Jones energy of the XPLOR energy terms.

complexed with NHE1 is well dispersed with favorable line shapes (Fig. 2), suggesting that the complex essentially adopts an ordered monomeric structure in solution.

Our target complex was ~27 kDa in size, assuming a 1:1 complex of CHP1 (22 kDa) and NHE1 (5 kDa). This represented a relatively large molecular weight in terms of conventional NMR studies. Consequently utilization of triple labeling (^{2}H, ^{13}C, and ^{15}N) and the recently developed computational methodology, CANDID, was extremely helpful in the structure determination. Sequential backbone assignments and most side-chain assignments were obtained from a 60% ^{2}H/^{15}N/^{13}C-labeled sample using standard triple resonance experiments. Missing ^{1}H resonances were supplemented using heteronuclear three-dimensional NOESY experiments with ^{15}N/^{13}C-labeled samples. Resonance assignments of methyl groups were carefully confirmed in a stereospecific manner using two-dimensional Constant Time HSQC spectra recorded for a 15% randomly enriched ^{13}C sample. Methyl groups for 18 of 24 leucines and nine of 11 valines were stereospecifically assigned. Aromatic ring proton assignments, essential for delineating hydrophobic core and protein-protein interactions, were obtained using two-dimensional TOCSY, two-dimensional NOESY, two-dimensional HCCH(arom) TOCSY, and three-dimensional ^{13}C(arom)-edited ^{15}N-separated NOESY experiments.

NMR spectra including the three-dimensional ^{13}C-edited NOESY spectrum used to monitor inter/intramolecular ^{1}H-^{1}H NOEs were of adequate quality to pursue a structural determination of the NHE1-CHP1 complex. Use of partial deuteration and the almost complete resonance assignment of methyl groups forming the hydrophobic core facilitated an initial determination of the overall protein fold. A high resolution structure was subsequently obtained using CANDID for automated assignments, which included the use of ambiguous NOEs from ^{15}N- and ^{13}C-edited NOESY experiments recorded for ^{15}N- or ^{15}N/^{13}C-labeled protein samples. An iterative approach was used for assigning NOEs in addition to the manually assigned unambiguous NOEs. The solution structure of the CHP1-NHE1 complex was determined from a total of over 4000 NMR-derived restraints, including 134 intermolecular distance restraints (Table 1). The ensemble of 20 structures in excellent agreement with a large body of experimental data were well defined (Fig. 3*A*). The r.m.s. deviations of backbone and heavy atoms over residues 518–537 of NHE1 and residues 10–92 and 108–193 of CHP1 were 0.53 and 1.15 Å, respectively. Of the NMR structures determined, the one with the smallest total energy was selected as representative for further discussion. The complex is predominantly α-helical, and the CHP1 helices constitute a cleft. A helix of the cytoplasmic region of NHE1 associates with CHP1 in 1:1 stoichiometry via the cleft (Fig. 3, *A* and *B*).

Structure of NHE1—NHE1 forms a five-turn amphipathic helix composed of residues 518–537. Orientation of the NHE1 helix is well defined relative to CHP1, consistent with the large

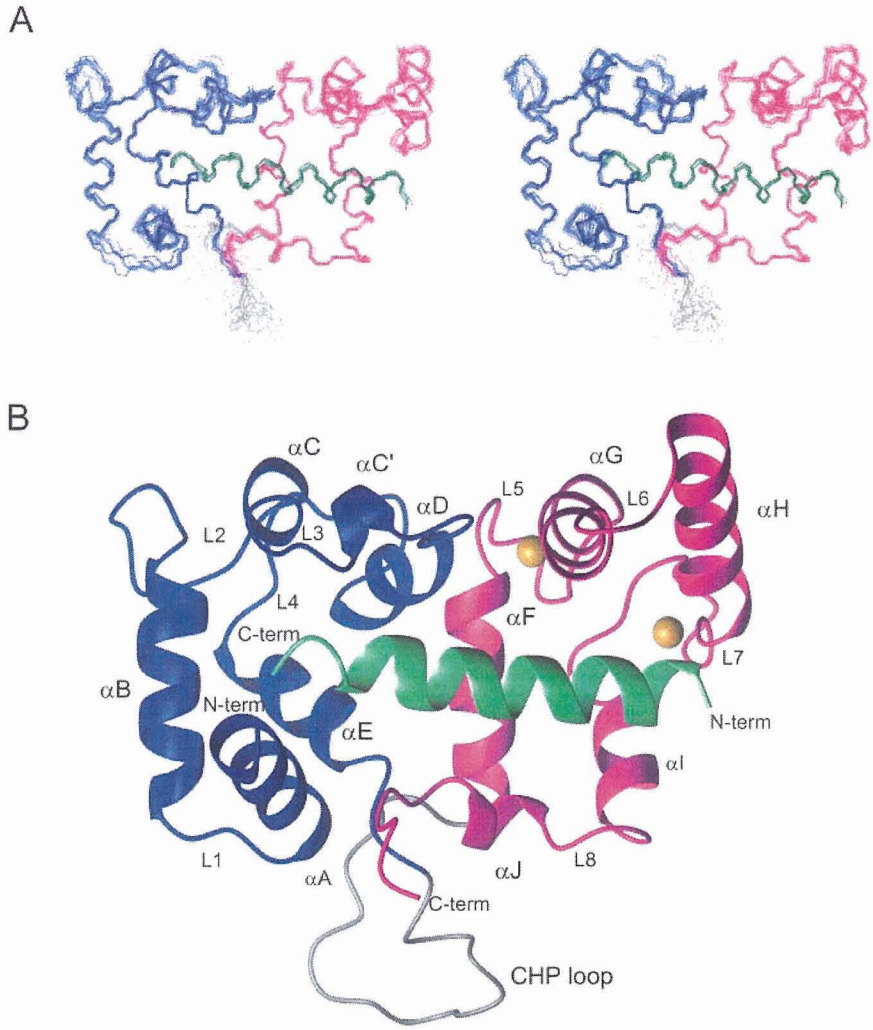

FIGURE 3. **Solution structure of the NHE1-CHP1 complex.** *A*, stereoview of the backbone superpositions of the final 20 simulated annealing structures of the NHE1-CHP1 complex. *B*, ribbon drawing of the representative NHE1-CHP1 structure complex. *A* and *B*, residues 517–538 of NHE1 and 10–192 of CHP1 are shown. The N- and C-terminal domains of CHP1 are colored in *blue* and *magenta*, respectively, and the CHP loop is colored in *gray*. NHE1 is shown in *green*. Ca^{2-} ions are shown by *gold spheres*.

number of intermolecular NOEs detected between CHP1 and NHE1 (Table 1 and Fig. 3*A*). The N-terminal half of the helix (residues 518–530) binds to the C-terminal domain of CHP1, and the C-terminal half of the helix (residues 531–537) binds to the N-terminal domain of CHP1 (Fig. 4*A*). Side-chain conformations of the helix are also well defined particularly for apolar residues that make extensive contacts with CHP1. For example, NMR spin-echo difference $^3J_{NC\gamma}$ and $^3J_{C'C\gamma}$ experiments, which bring about $\chi 1$ rotamer information of aromatic side chain, showed that the His-523 and Phe-526 adopted *g*+ and *t* conformations, respectively. The helix exhibits amphipathic character in which the bulky hydrophobic residues Ile-518, Ile-522, His-523, Phe-526, Leu-527, Leu-530, Leu-531, Ile-534, and Ile-537 are clearly confined to one side, and hydrophilic residues are exposed at the other side (Fig. 4*B*). The hydrophobic residues form a continuous apolar surface (Fig. 4*B*). The main-chain and side-chain conformations of residues preceding and following the helix, residues 503–517 and 538–545, respectively, are poorly defined in the NMR structure because of the absence of medium and long range NOEs involving these regions. The narrow resonance linewidths, chemical shift index, and steady state $\{^1H\}$-^{15}N heteronuclear NOE suggest that these regions are unstructured in the complex.

Structure of CHP1—CHP1 is composed of 10 α-helices and a long loop folded into two globular regions representing the N- and C-terminal domains (Fig. 3*B*). The secondary structure consists of αA (residues 11–22), αB (residues 26–37), αC (residues 48–51), αD (residues 64–70), αE (residues 80–88), αF (residues 111–122), αG (residues 132–143), αH (residues 149–162), αI (residues 174–180), and αJ (residues 185–188) (Figs. 1*B* and 3*B*). The N-terminal domain consists of ancestral EF-hands, EF-1 and EF-2, that do not bind calcium under physiological conditions. The EF-1 hand includes helix αB, loop L2, and helix αC followed by loop L3 to the second EF-hand that includes helix αD, loop L4, and helix αE (Figs. 1*B* and 3*B*). A long loop region consisting of residues 93–110 connects the N- and C-terminal domains. Because this characteristic long insertion is not found in calcineurin B (Figs. 1*B* and 3, *A* and *B*), we refer to this long loop as the CHP loop. The absence of medium and long range NOEs, a chemical shift index, and $\{^1H\}$-^{15}N heteronuclear NOE value indicate that this region is flexible in solution. The first EF-hand in the C-terminal domain includes helix αF, loop L5, and helix αG followed by loop L6 and the second EF-hand that consists of helix αH, loop L7, and helix αI (Figs. 1*B* and 3*B*).

The four CHP1 EF-hands form a deep hydrophobic pocket, which constitutes the interaction surface for the NHE1 amphipathic α-helix. CHP1 binds to the apolar side of NHE1 with the four EF-hands through a side-by-side manner (Fig. 4*A*). This contrasts with the well known canonical CaM-target binding mode that represents a wrap-around manner in which two pairs of EF-hands bind to the target IQ motif helix on opposite sides to each other (43, 44).

Although there is modest sequence similarity between CHP1 and CaM, it should be noted that the latter interacts with a large number of proteins with various interaction modes including canonical 1:1 binding and non-canonical 1:1, 1:2, and 2:2 binding (43, 44). It has been suggested that the observed binding versatility of CaM could be derived from the variable positioning of the two domains, linked by a flexible linker, that can

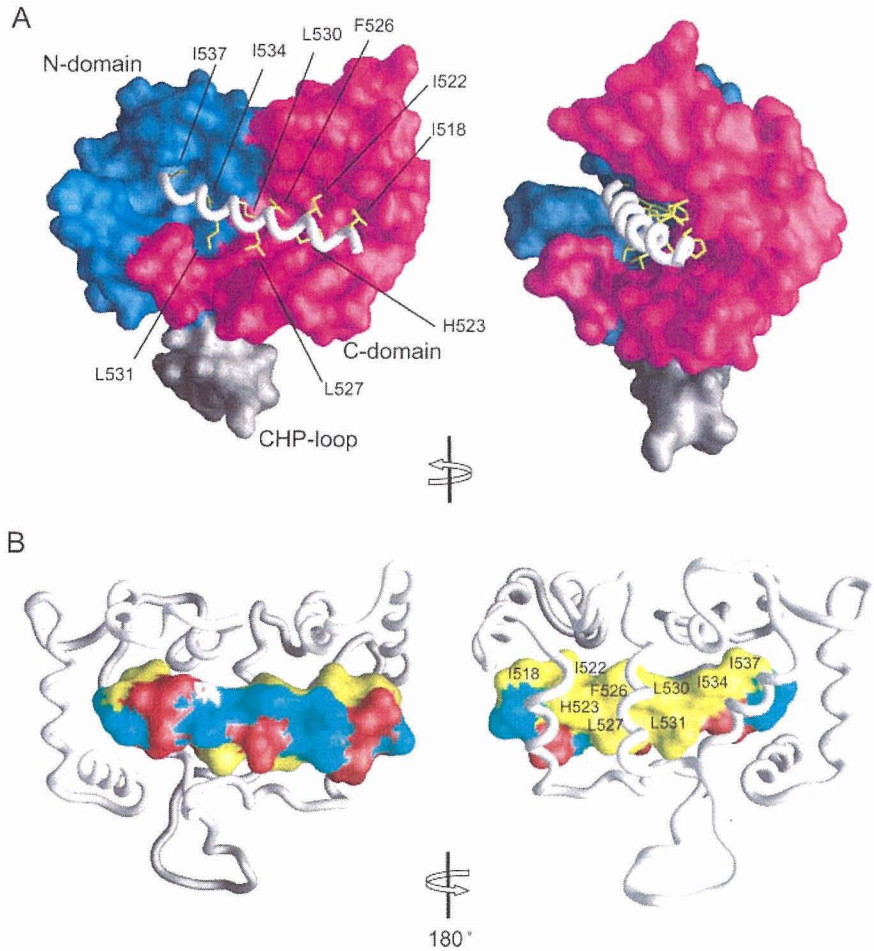

FIGURE 4. **Molecular surface of the NHE1-CHP1 complex.** *A*, molecular surface of CHP1 and backbone *tube* representation of NHE1 with *yellow stick* that shows the hydrophobic side chains. The N- and C-terminal domains of CHP1 are colored in *blue* and *magenta*, respectively. *B*, molecular surface of NHE1 and backbone *tube* representation of CHP1. Hydrophobic, acidic, and polar residues are colored in *yellow*, *red*, and *blue*, respectively.

accommodate different targets. Although target multiplicity has been reported in the case of CHP1, it seems to possess more limited binding modes than CaM. One notable feature of CHP1 that illustrates its difference to CaM has to do with the interdomain interaction. This interaction restricts domain orientation, a phenomenon absent in CaM. In our CHP1 structure, residue Leu-62 of the N-terminal domain participates in a hydrophobic interaction with residues Val-138 and Met-141 of the C-terminal domain, and residue Ala-69 of the N-terminal domain interacts with residue Leu-122 of the C-terminal domain. A side-by-side interaction mediated by four EF-hands has also been reported to take place with voltage-gated potassium channel (Kv)-interacting protein (KChIP) (45) and with CNA-CNB (46, 47) (Fig. 5*A*).

The atomic r.m.s. difference of well fitted parts between CHP1 complexed with NHE1 and CNB complexed with CNA (Protein Data Bank code 1AUI) is 2.7 Å, indicating that the fit is not very good, although the topology is identical with a high Z-score of 11.8 from a distance matrix alignment (DALI) search. The r.m.s. deviation value improves to 1.7 Å when only the N-terminal domains are superimposed, and it is 1.8 Å when only the C-terminal domains are superimposed. This indicates that the higher r.m.s. deviation for both domains originates from an interdomain swiveling between NHE1-CHP1 and CNA-CNB, although both proteins bind cognate targets in a side-by-side manner. Similarly domain swiveling was observed between NHE1-bound and NHE-free CHP1. Swiveling of the N- and C-terminal domains could create a binding surface for cognate targets.

Comparison with Other EF-hands—It is interesting to note that both EF-1 and EF-2 adopt an open conformation in NHE1-bound CHP1 without Ca^{2+}. This is especially evident when comparing the angles between the EF-hand helices. In Fig. 5*B*, a graphical view of the interhelical angles between the first and second helices of EF-1 and EF-2 of apoCaM (a typical closed conformation), Ca^{2+}-CaM (a typical open conformation, CNB), KChIP1, NHE1-bound CHP1, and NHE1-free CHP1 is displayed using a vector geometry mapping method (48, 49). The first helices of the EF-hands are superimposed along the *z* axis, and the spatial localization of the second helices are shown as a *cylinder*. This indicates that both EF-1 and EF-2 of NHE1-bound CHP1 adopt an open conformation, whereas EF-1 and EF-2 of NHE1-free CHP1 adopt an open and semiopen conformation, respectively (Fig. 5*B* and supporting information S1). This implies that EF-1 and EF-2 adopt a constitutively open conformation. However, it should be noted that the hydrophobic cleft of the N-terminal domain of free CHP1, as revealed by the crystal structure, is plugged by additional linker residues (Leu-Ala-Ala-Ala-Leu-Glu-His) (23) derived from the expression vector, partly mimicking the NHE1 helix (Fig. 5*A*). Binding of the vector-derived linker might have facilitated adoption of the open and semiopen conformations of EF-1 and EF-2, respectively. Therefore, the possibility of a "closed to open" conformational transition of EF-1 and EF-2 remains to be evaluated.

The binding of EF-hands in an open conformation without Ca^{2+} to target molecules has been found following crystal structure investigations of a Kv-KChIP1 in which the Kv fragment is covalently linked to the C terminus of KChIP1 (45). In this case, the Kv fragment binds to EF-1 and EF-2 of the N-terminal domain of KChIP1 through hydrophobic interactions (Fig. 5*A*). Of particular note, KChIP1 forms a dimer utilizing the surface formed by the Kv peptides and helix 10 of the C-terminal domain of KChIP1 in contrast to NHE1-CHP1, which exists as a monomer (Fig. 5*C*). The interhelix angles of EF-1 and EF-2

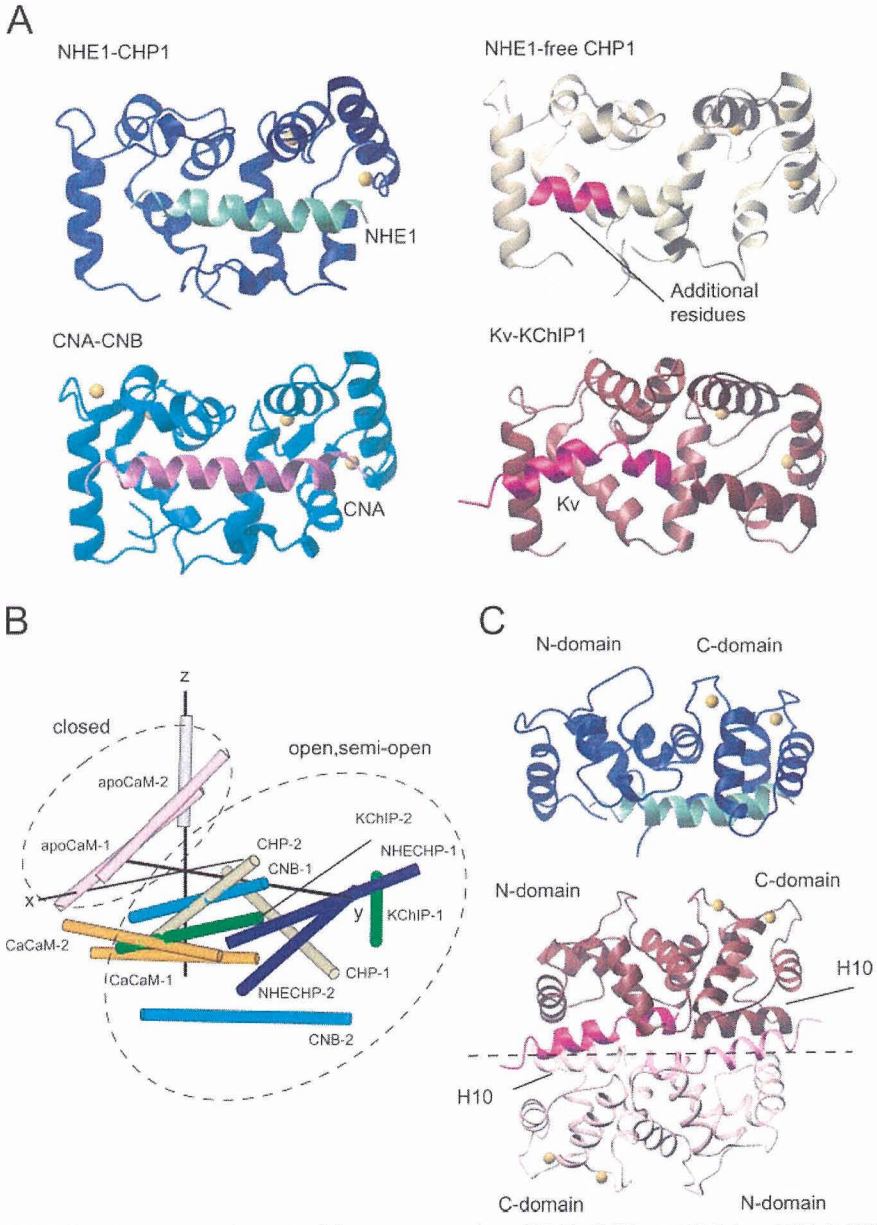

FIGURE 5. **Structure comparisons.** *A*, ribbon representation of NHE1-CHP1, rat NHE1-free CHP1 (2CT9) in which additional residues from the expression vector interacting with the N-terminal domain (LAAALEH) are depicted in *magenta*, CNA-CNB (1AUI), and Kv-KChIP1 (1S6C). Protein Data Bank entries are shown in parentheses. *B*, vector geometry mapping of EF-1 and EF-2 apocalmodulin, Ca^{2+}-calmodulin, calcineurin B, Kv-KChIP1, NHE1-bound CHP1, and NHE1-free CHP1 are denoted as "*apoCaM*," "*CaCaM*," "*CNB*," "*KChIP*," "*NHECHP*," and "*CHP*," respectively. *Hyphenated numbers 1* and *2* denote EF-1 and EF-2, respectively, for each protein. *C*, comparison of the KChIP1 dimer and CHP1 structures colored in *brown* and *blue*, respectively. Bound Kv and NHE1 are colored in *pink* and *green*, respectively. The dimer interface of KChIP1 is shown as a *dashed line*, and one molecule of the dimer is shown in *light colors*. KChIP1 and CHP1 are depicted in the same orientation. In *A* and *C*, the N- and C-terminal regions, αA, and the CHP loop of CHP1 are not shown in the comparison for reasons of clarity.

are 82° and 72°, respectively (supporting information S1), which are slightly larger than those of CHP1. A dimeric interaction in addition to binding of the Kv fragment may contribute to broadening of the cleft constituted by EF-1 and EF-2.

CHP1 shares 18% sequence identity with KChIP1, and the folding topology is almost identical (Fig. 5*A*). However, the target recognition mechanism differs from that of KChIP1 as judged from the determined structures. KChIP1 belongs to the extensively studied NCS1 family, which act as important regulators of various functions among certain higher eukaryotes (50). We propose that the NHE1-CHP1 interaction represents a novel binding mode utilized throughout the four-EF-hand proteins, which constitute a distinct subfamily to the NCS1 family. Furthermore detailed comparison of the binding mode of CHP1 and CNB will be presented below.

The CHP1-NHE1 Interface—The protein-protein interface consists of an extensive hydrophobic concave CHP1 undersurface and an apolar NHE1 surface. The concave undersurface spans both the N- and C-terminal domains of CHP1. The total surface area buried at the interface is 2338 $Å^2$, slightly smaller than the value of 2625 $Å^2$ for the interface between CNA and CNB (Protein Data Bank code 1AUI). Approximately more than 90% of the total buried surface area between NHE1 and CHP1 is hydrophobic, similar to the complexed structure of CNA and CNB.

The interface formed between NHE1 and CHP1 includes methyl-containing and aromatic hydrophobic residues. The residues of the N-terminal domain of CHP1, Ala-69, Phe-90, Ile-66, Thr-86, Leu-87, Phe-35, and Leu-54, comprise a hydrophobic cleft that interacts with the apolar surface formed by the side chains of NHE1 residues Leu-530, Ile-534, and Ile-537. Additionally the side chain of NHE1 Leu-531 expands the hydrophobic area interacting with CHP1 Phe-90 (Fig. 6*A*). The C-terminal domain residues of CHP1, Ala-163, Thr-159, Leu-139, Leu-135, Tyr-122, Phe-176, Ile-171, Phe-117, Ala-118, and Leu-121, constitute a continuous hydrophobic cleft that interacts with the N-terminal portion of NHE1 helix residues Ile-518, Ile-522, and Phe-526, which protrude at the apolar side. NHE1 residues Leu-527 and His-523 make additional hydrophobic contact with CHP1 residues Tyr-122, Phe-176, and Val-185 (Fig. 6*A*). These interface-forming hydrophobic residues are well conserved within NHE and CHP isoforms, reflecting the importance of these interactions (Fig. 1*B*). Furthermore the acidic side chain of Asp-528 at the center of NHE1 helix seems to form a salt bridge with the basic side

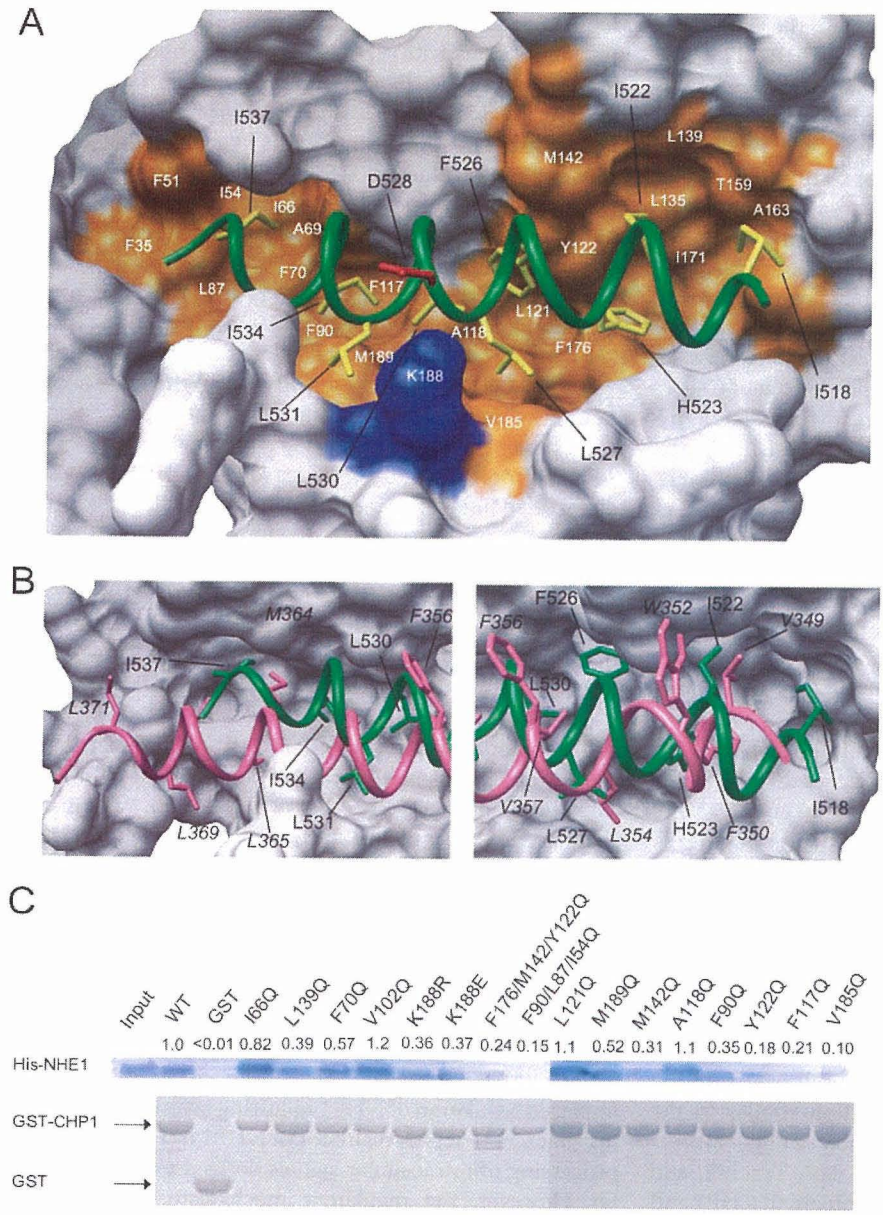

FIGURE 6. **Noncovalent interactions at the NHE1-CHP1 interface and contribution to the overall stability of the complex.** *A*, molecular surface of CHP1 and backbone *tube* representation of NHE1 with *yellow* and *red sticks* that show hydrophobic and acidic side chains, respectively. Hydrophobic and basic surface residues of CHP1 are colored in *orange* and *blue*, respectively. *B*, superposition of NHE1-CHP1 and CAN-CNB (Protein Data Bank code 1AUI). NHE1 and CNA are shown in *green* and *magenta*, respectively, and the molecular surface of only CHP1 is depicted for clarity. Complex-forming hydrophobic residues of NHE1 and CNA are shown as *sticks* and are labeled. CNA residues are represented in *italics*. The *left-hand image* and the *right-hand image* are close-up views of the N- and C-terminal domains. *C*, binding of His-NHE1 peptide to GST-CHP1 mutants in an *in vitro* pulldown assay. Bound peptide was separated via SDS-PAGE, blotted to a membrane, and then visualized using Ni-NTA-conjugated alkaline phosphatase (*top*). The amount of GST-CHP1 mutant used was estimated by Coomassie Blue staining (*bottom*) for calibration. The binding of NHE1 peptide to GST-CHP1 mutants was quantified and expressed as a ratio of binding of wild-type protein at the *top* of the gel images.

chain of CHP1 Lys-188. The presence of this interaction was observed in 10 of the final 20 NMR structures derived using the MONSTER server (51), which identifies interacting residues and assigns the nature of those interactions based on the structure. These residues are also conserved (Figs. 1, *A* and *B*, and 6*A*).

NHE1 binding orientation relative to CHP1 is probably established by surface complementarity that comprises the hydrophobic surfaces of NHE1 and CHP1. NHE1 side chains of Ile-534 and Ile-537 protrude into the shallow cleft made by the CHP1 N-terminal domain. Meanwhile NHE1 aromatic side chains of His-523 and Phe-526 protrude into the deep cleft of the CHP1 C-terminal domain (Fig. 6*A*). This deep cleft allows enough space so that they can interact with the bulky side chains of NHE1. The difference between the shapes of the domains is critical for NHE1 binding orientation.

Notably the shape of the interaction surfaces of NHE1-CHP1 and CNA-CNB differs. The spatial arrangement of NHE1 and CNA residues that contribute to form the interaction surfaces differs for each (Fig. 6*B*). Only Val-349, Phe-350, and Val-357 of CNA are located at equivalent positions to Ile-522, His-523, and Leu-530 of NHE1 unlike other residues. Cleary Trp-352 and Phe-356 of CNA that interact with the roof of the hydrophobic cleft formed by CNB are missing in NHE1. Furthermore the interactions mediated by the C-terminal stretch region of CNA, where Leu-369 and Leu-371 protrude, are absent in NHE1. On the other hand, the corresponding residues to Phe-526 and Ile-518 of NHE1 are absent in CNA.

Consequently the interaction mechanism dominated by hydrophobic interactions through amphipathic helices and four EF-hands is common in both complexes, but their shape differs. This surface complementarity in terms of a knobs-into-hole mode of interaction defines the binding specificity of these proteins, although the folding topology is identical.

Correlation with Mutagenesis Studies—The solution structure of the CHP1-NHE1 complex is essentially consistent with previous mutagenesis studies concerning NHE1. Co-immunoprecipitation experiments showed that the 4Q mutant of NHE1, in which Phe-526, Leu-527, Leu-530, and Leu-531 are substituted with glutamine, displayed no binding to CHP1, whereas the I518Q/I522Q NHE1 double mutant displayed some binding albeit with decreased affinity (3). Our structure determination revealed that Phe-526, Leu-527, Leu-530, and Leu-531 form a hydrophobic core that interacts with the center of the hydrophobic cleft of the C-terminal domain of

CHP1, whereas Ile-518 and Ile-522 interact with the rim of the hydrophobic cleft of the C-terminal domain of CHP1 (Figs. 4*B* and 6*A*). Deletion mutagenesis indicated that NHE1 (residues 510–575) retained binding affinity similar to the wild-type protein, implying that the juxtamembrane region of NHE1 comprising residues 503–509 is unimportant for CHP1 binding (3). These residues were found to be unstructured in the present study and form no direct contact with NHE1.

The binding activity of NHE1 (residues 530–656) lacking the N-terminal segment was found to be completely impaired (3). Our NHE1-CHP1 complex structure shows that an absence of residues preceding Leu-530 results in almost complete loss of interaction between NHE1 and the C-terminal domain of CHP1, whereas the many hydrophobic interactions mediated by NHE1 residues Leu-530, Leu-531, Ile-534, and Ile-537 are retained (Fig. 6*A*). This indicates that interaction of the N-terminal residues of NHE1 and the C-terminal domain of CHP1 is indispensable in maintaining the NHE1-CHP1 complex. Namely this part of the interaction plays a dominant role in NHE1-CHP1 complex formation.

CHP1 was subjected to site-directed mutagenesis in an effort to reveal detailed individual contributions of interfacial residues toward the overall stability of the NHE1-CHP1 complex. We selected three categories of residues in CHP1: 1) residues that comprise the floor of the hydrophobic pocket, Phe-70, Phe-90, Phe-117, Ala-118, Leu-121, Tyr-122, and Met-189; 2) residues forming the rim of the pocket, Ile-66, Leu-139, Met-142, and Val-185; and 3) a residue forming the salt bridge, Lys-188. A noninteracting solvent-exposed residue, Val-102, as the positive control and a triple mutation involving hydrophobic residues Phe-90/Leu-87/Leu-54 and Phe-176/Met-142/Tyr-122 as the negative control were prepared.

Dramatic effects were observed in terms of CHP1 binding to NHE1 with mutations F117Q, Y122Q, and V185Q (Fig. 6*C*). We expected the floor-forming residues located at the bottom of the cleft to be critical for the interaction, but the rim-forming residue Val-185 showed significant reduction similar to the negative control. Based on the solution structure of the NHE1-CHP1 complex, it was appeared that Phe-117, Tyr-122, and Val-185 were confined to the C-terminal domain of CHP1 and were packed against the apolar side of NHE1. This suggests that the C-terminal hydrophobic cleft represents a mutation hot spot, implying that it plays a key role in the NHE1-CHP1 interaction. This result is consistent with the NHE1 deletion result indicating that interaction between the N-terminal segment of NHE1 and the C-terminal domain of CHP1 is dominant. This represents a unique feature of the NHE1-CHP1 interaction.

Although mutation of residues possibly involved in salt bridge formation such as K188E and K188R resulted in a marked decrease in binding interaction, the effect was not strong, and the charge-reversing effect of K188E was unclear. Thus, it appears that although this salt bridge contributes to NHE1-CHP1 complex formation, it is not the main force possibly because this bond is exposed to solvent (Fig. 6*A*), and therefore solvation could weaken the strength of the interaction.

Role of CHP1—NMR investigations of NHE1 complexed with CHP1 revealed that the juxtamembrane region comprising residues 503–517 was unstructured in solution. This region is rich in basic residues with a previous study reporting that NHE1 comprising residues 506–576 bound to PIP_2 *in vitro* (13). In addition, residues 513–520 and 556–564 might represent PIP_2 binding sites (13). Accordingly it is likely that this juxtamembrane region (residues 503–517) following the last transmembrane helix (H12, residues 478–499) is incapable of forming a continuous straight helical structure into the cytoplasm due to interaction with the membrane. Rather the overall structure of NHE1 presumably turns or bends toward the cytoplasmic membrane following a PIP_2-mediated interaction. Assuming that flanking regions of the helix, residues 513–520 and 556–564, attach to the membrane (PIP_2) (13), the helix and CHP1 should be located immediately beneath the cytoplasmic membrane.

Furthermore it has been reported that NHE1 acts as a scaffold protein linked to actin filaments via ezrin-radixin-moesin proteins in addition to possessing function as an ion exchanger (52, 53). Our NMR studies revealed that the cytoplasmic helix-forming residues of NHE1 comprise residues 518–537, which showed little overlap from the previously reported ezrin-radixin-moesin binding region (512–520 and 550–565). This ensures simultaneous binding of NHE1 to CHP1 and ezrin-radixin-moesin proteins.

The juxtamembrane region of NHE1 forms a particular tertiary or quaternary structure that is mediated by interactions with the membrane (PIP_2), CHP1, and ezrin-radixin-moesin proteins. The overall structure of the juxtamembrane region might play an important role in NHE1 activity. The 90% loss in activity following CHP1 depletion might be due to disruption of the structure of the cytoplasmic region of NHE1 around the membrane. In fact, although this represents *in vitro* evidence, the amphipathic helix is disrupted in the absence of CHP1 based on the CD and NMR data (supporting information S2 and S3).

Possible Mode of Regulation—CHP1 deprivation resulted in impaired regulation of NHE1 following external stimuli, implying that CHP1 acts as regulator of NHE1 by involvement in the processing of intracellular signals derived from external stimuli. However, the regulatory mechanism remains unclear. Although it was reported that CHP1 is an *N*-myristoylated protein, CHP1 does not exert myristoyl switching in a Ca^{2+}-dependent manner under normal physiological conditions because EF-3 and EF-4 constitutively bind Ca^{2+} ions where *N*-myristoylation was not required for NHE1 binding, activation, or localization (14).

Of particular note, it was reported that CHP1 is a phosphorylated protein, although the phosphorylation sites were not determined. According to the phosphorylation prediction server NetPhos (54), the CHP1 sequence contains potential phosphorylation sites located at residues Thr-36, Ser-37, Ser-47, Ser-131, and Ser-172 (score, >0.8). Similarly the phosphorylation server Scansite (55) identified potential phosphorylation sites located at residues Thr-36, Ser-37, and Ser-172 (score, >0.5). From the determined NHE1-CHP1 structure, residues Thr-36, Ser-37, and Ser-172, predicted by both servers as potential phosphorylation sites, are locate at the terminal part of the EF-hand helix or its flanking loop where the side chains of

the aforementioned residues are exposed to the protein surface reinforcing the possibility of phosphorylation. Phosphorylation-induced conformational changes in CHP1 and the subsequent regulation of NHE1 activity are interesting areas that remain to be investigated.

Conclusion—We have determined the solution structure of the cytoplasmic region of NHE1 complexed with CHP1. Although previous biochemical analyses suggested that the hydrophobic residues of NHE1 were likely to interact with CHP1, the present study has delineated the structural basis for this interaction. The solution structure provides concrete evidence that the cytoplasmic region of NHE1 forms an amphipathic helix that interacts directly with the large concave undersurface of CHP1. This helix is disrupted in the absence of CHP1; thus the loss in activity following CHP1 depletion might be due to disruption of the structure of the juxtamembrane region of NHE1. Our structure provides a first step toward understanding the regulation of NHE1 activity. Moreover it revealed a novel target binding mechanism mediated by four EF-hands. These findings should facilitate future studies aimed at understanding the mechanism underlying recognition utilized by EF-hand proteins that are engaged in signal transduction pathways and many other molecular and cellular events. During the initial review of our manuscript, a study appeared that describes a crystal structure of the NHE1 peptide complexed with CHP2 containing Y^{3+} ions instead of Ca^{2+} (56).

Acknowledgments—We are grateful to Momoko Yoneyama, Hiroko Kinoshita, and Junko Tsukamoto of the Nara Institute of Science and Technology for technical assistance and Kokoro Hayashi for help in sample preparation.

REFERENCES

1. Orlowski, J., and Grinstein, S. (2004) *Pfluegers Arch. Eur. J. Physiol.* **447,** 549–565
2. Lin, X., and Barber, D. L. (1996) *Proc. Natl. Acad. Sci. U. S. A.* **93,** 12631–12636
3. Pang, T., Su, X., Wakabayashi, S., and Shigekawa, M. (2001) *J. Biol. Chem.* **276,** 17367–17372
4. Bertrand, B., Wakabayashi, S., Ikeda, T., Pouyssegur, J., and Shigekawa, M. (1994) *J. Biol. Chem.* **269,** 13703–13709
5. Wakabayashi, S., Bertrand, B., Ikeda, T., Pouyssegur, J., and Shigekawa M. (1994) *J. Biol. Chem.* **269,** 13710–13715
6. Dhanasekaran, N., Prasad, M. V., Wadsworth, S. J., Dermott, J. M., and van Rossum, G. (1994) *J. Biol. Chem.* **269,** 11802–11806
7. Hooley, R., Yu, C. Y., Symons, M., and Barber, D. L. (1996) *J. Biol. Chem.* **271,** 6152–6158
8. Voyno-Yasenetskaya, T., Conklin, B. R., Gilbert, R. L., Hooley, R., Bourne, H. R., and Barber, D. L. (1994) *J. Biol. Chem.* **269,** 4721–4724
9. Bianchini, L., L'Allemain, G., and Pouyssegur, J. (1997) *J. Biol. Chem.* **272,** 271–279
10. Takahashi, E., Abe, J., Gallis, B., Aebersold, R., Spring, D. J., Krebs, E. G., and Berk, B. C. (1999) *J. Biol. Chem.* **274,** 20206–20214
11. Lehoux, S., Abe, J.-i., Florian, J. A., and Berk, B. C. (2001) *J. Biol. Chem.* **276,** 15794–15800
12. Yan, W., Nehrke, K., Choi, J., and Barber, D. L. (2001) *J. Biol. Chem.* **276,** 31349–31356
13. Aharonovitz, O., Zaun, H. C., Balla, T., York, J. D., Orlowski, J., and Grinstein, S. (2000) *J. Cell Biol.* **150,** 213–224
14. Pang, T., Hisamitsu, T., Mori, H., Shigekawa, M., and Wakabayashi, S. (2004) *Biochemistry* **43,** 3628–3636
15. Barroso, M. R., Bernd, K. K., DeWitt, N. D., Chang, A., Mills, K., and Sztul, E. S. (1996) *J. Biol. Chem.* **271,** 10183–10187
16. Lin, X., Sikkink, R. A., Rusnak, F., and Barber, D. L. (1999) *J. Biol. Chem.* **274,** 36125–36131
17. Timm, S., Titus, B., Bernd, K., and Barroso, M. (1999) *Mol. Biol. Cell* **10,** 3473–3488
18. Matsumoto, M., Miyake, Y., Nagita, M., Inoue, H., Shitakubo, D., Takemoto, K., Ohtsuka, C., Murakami, H., Nakamura, N., and Kanazawa, H. (2001) *J. Biochem. (Tokyo)* **130,** 217–225
19. Nakamura, N., Miyake, Y., Matsushita, M., Tanaka, S., Inoue, H., and Kanazawa, H. (2002) *J. Biochem. (Tokyo)* **132,** 483–491
20. Pang, T., Wakabayashi, S., and Shigekawa, M. (2002) *J. Biol. Chem.* **277,** 43771–43777
21. Mailander, J., Muller-Esterl, W., and Dedio, J. (2001) *FEBS Lett.* **507,** 331–335
22. Perera, E. M., Martin, H., Seeherunvong, T., Kos, L., Hughes, I. A., Hawkins, J. R., and Berkovitz, G. D. (2001) *Endocrinology* **142,** 455–463
23. Naoe, Y., Arita, K., Hashimoto, H., Kanazawa, H., Sato, M., and Shimizu, T. (2005) *J. Biol. Chem.* **280,** 32372–32378
24. Yamazaki, T., Lee, W., Arrowsmith, C. H., Muhandiram, D. R., and Kay, L. E. (1994) *J. Am. Chem. Soc.* **116,** 11655–11666
25. Matsuo, H., Kupce, E., Li, H., and Wagner, G. (1996) *J. Magn. Reson. B* **111,** 194–198
26. Muhandiram, D. R., and Kay, L. E. (1994) *J. Magn. Reson. B* **103,** 203–216
27. Clowes, R. T., Boucher, W., Hardman, C. H., Domaille, P. J., and Laue, E. D. (1993) *J. Biomol. NMR* **3,** 349–354
28. Kay, L. E., Xu, G. Y., Singer, A. U., Muhandiram, D. R., and Formankay, J. D. (1993) *J. Magn. Reson. B* **101,** 333–337
29. Logan, T. M., Olejniczak, E. T., Xu, R. X., and Fesik, S. W. (1993) *J. Biomol. NMR* **3,** 225–231
30. Neri, D., Szyperski, T., Otting, G., Senn, H., and Wuthrich, K. (1989) *Biochemistry* **28,** 7510–7516
31. Boucher, W., Laue, E. D., Campbell-Burk, S., and Domaille, P. J. (1992) *J. Am. Chem. Soc.* **114,** 2262–2264
32. Cavanagh, J., Fairbrother, W. J., Palmer, A. G., III, and Skelton, N. J. (1996) *Protein NMR Spectroscopy*, pp. 301–531, Academic Press, San Diego, CA
33. Grzesiek, S., and Bax, A. (1993) *J. Biomol. NMR* **3,** 185–204
34. Delaglio, F., Grzesiek, S., Vuister, G. W., Zhu, G., Pfeifer, J., and Bax, A. (1995) *J. Biomol. NMR* **6,** 277–279
35. Goddard, T. D., and Kneller, D. G. (1999) *SPARKY3*, University of California, San Francisco
36. Herrmann, T., Guntert, P., and Wuthrich, K. (2002) *J. Mol. Biol.* **319,** 209–227
37. Schwieters, C. D., Kuszewski, J. J., Tjandra, N., and Clore, G. M. (2003) *J. Magn. Reson.* **160,** 65–73
38. Laskowski, R. A., Rullmannn, J. A., MacArthur, M. W., Kaptein, R., and Thornton, J. M. (1996) *J. Biomol. NMR* **8,** 477–486
39. Koradi, R., Billete, M., and Wuthrich, K. (1996) *J. Mol. Graph.* **14,** 51–55
40. Nicholls, A., Sharp, K. A., and Honig, B. (1991) *Proteins Struct. Funct. Genet.* **11,** 281–296
41. Pettersen, E. F., Goddard, T. D., Huang, C. C., Couch, G. S., Greenblatt, D. M., Meng, E. C., and Ferrin, T. E. (2004) *J. Comput. Chem.* **25,** 1605–1612
42. Goda, N., Tenno, T., Takasu, H., Hiroaki, H., and Shirakawa, M. (2004) *Protein Sci.* **13,** 652–658
43. Hoeflich, K. P., and Ikura, M. (2002) *Cell* **108,** 739–742
44. Bhattacharya, S., Bunick, C. G., and Chazin, W. J. (2004) *Biochim. Biophys. Acta* **1742,** 69–79
45. Zhou, W., Qian, Y., Kunjilwar, K., Pfaffinger, P. J., and Choe, S. (2004) *Neuron* **41,** 573–586
46. Griffith, J. P., Kim, J. L., Kim, E. E., Sintchak, M. D., Thomson, J. A., Fitzgibbon, M. J., Fleming, M. A., Caron, P. R., Hsiao, K., and Navia, M. A. (1995) *Cell* **82,** 507–522
47. Kissinger, C. R., Parge, H. E., Knighton, D. R., Lewis, C. T., Pelletier, L. A., Tempczyk, A., Kalish, V. J., Tucker, K. D., Showalter, R. E., Moomaw, E. W., Gastinel, L. N., Habuka, N., Chen, X., Maldonado, F., Barker, J. E., Bacquet, R., and Villafranca, J. E. (1995) *Nature* **378,** 641–644
48. Yap, K. L., Ames, J. B., Swindells, M. B., and Ikura, M. (1999) *Proteins* **37,**

499–507
49. Yap, K. L., Ames, J. B., Swindells, M. B., and Ikura, M. (2002) *Methods Mol. Biol.* **173,** 317–324
50. Burgoyne, R. D., and Weiss, J. L. (2001) *Biochem. J.* **353,** 1–12
51. Salerno, W. J., Seaver, S. M., Armstrong, B. R., and Radhakrishnan, I. (2004) *Nucleic Acids Res.* **32,** W566–W568
52. Baumgartner, M., Patel, H., and Barber, D. L. (2004) *Am. J. Physiol.* **287,** C844–C850
53. Denker, S. P., Huang, D. C., Orlowski, J., Furthmayr, H., and Barber, D. L. (2000) *Mol. Cell* **6,** 1425–1436
54. Blom, N., Gammeltoft, S., and Brunak, S. (1999) *J. Mol. Biol.* **294,** 1351–1362
55. Obenauer, J. C., Cantley, L. C., and Yaffe, M. B. (2003) *Nucleic Acids Res.* **31,** 3635–3641
56. Ammar, Y. B., Takeda, S., Hisamitsu, T., Mori, H., and Wakabayashi, S. (2006) *EMBO J.* **25,** 2315–2325